Light scattering by dust and anthropogenic aerosol at a remote site in the Negev desert, Israel

Tracey W. Andreae, Meinrat O. Andreae, and Charles Ichoku[1]
Biogeochemistry Department, Max Planck Institute for Chemistry, Mainz, Germany

Willy Maenhaut and Jan Cafmeyer
Institute for Nuclear Sciences, University of Gent, Gent, Belgium

Arnon Karnieli and Leah Orlovsky
Jacob Blaustein Institute for Desert Research, Ben Gurion University of the Negev, Israel

Received 15 August 2000; revised 4 June 2001; accepted 7 June 2001; published 16 January 2002.

[1] We investigated aerosol optical properties, mass concentration, and chemical composition over a 2 year period at a remote site in the Negev desert, Israel (Sde Boker, 30° 51′N, 34° 47′E, 470 m above sea level). Light-scattering measurements were made at three wavelengths (450, 550, and 700 nm), using an integrating nephelometer, and included the separate determination of the backscatter fraction. Aerosol coarse and fine fractions were collected with stacked filter units; mass concentrations were determined by weighing, and the chemical composition by proton-induced X-ray emission and instrumental neutron activation analysis. The total scattering coefficient at 550 nm showed a median of 66.7 Mm^{-1}(mean value 75.2 Mm^{-1}, standard deviation 41.7 Mm^{-1}) typical of moderately polluted continental air masses. Values of 1000 $Mm^{-1}$and higher were encountered during severe dust storm events. During the study period, 31 such dust events were detected. In addition to high scattering levels, they were characterized by a sharp drop in the Ångström coefficient (i.e., the spectral dispersion of the light scattering) to values near zero. Mass-scattering efficiencies were obtained by a multivariate regression of the scattering coefficients on dust, sulfate, and residual components. An analysis of the contributions of these components to the total scattering observed showed that anthropogenic aerosol accounted for about 70% of scattering. The rest was dominated by the effect of the large dust events mentioned above and of small dust episodes typically occurring during midafternoon. *INDEX TERMS:* 0305 Atmospheric Composition and Structure: Aerosols and particles (0345, 4801), 0345 Atmospheric Composition and Structure: Pollution—urban and regional (0305), 0360 Atmospheric Composition and Structure: Transmission and scattering of radiation

1. Introduction

[2] The factors affecting the Earth's radiation budget and, consequently, global climate have received considerable attention in recent years. While the effects of greenhouse gases are now fairly well understood, the climatic impact of atmospheric aerosols is still subject to large uncertainties [*Houghton et al.*, 1996; *Shine and Forster*, 1999; *Penner et al.*, 2001]. The global mean radiative forcing due to the long-lived "greenhouse" gases (carbon dioxide, methane, nitrous oxide, and halocarbons) is estimated to be +2.4 ± 0.2 W m^{-2}, and the confidence level of this estimate is rated as "high" [*Chanin*, 1996; *Houghton et al.*, 1996; *Shine and Forster*, 1999]. In contrast, the total global radiative forcing due to the direct and indirect effects of atmospheric aerosols is thought to be about −1.3 W m^{-2} with an uncertainty of at least a factor of 2 and a confidence level of "very low" [*Shine and Forster*, 1999]. The upper bound of the uncertainty range for aerosol radiative forcing implies even the possibility of a net global forcing of zero [*Houghton and Ding*, 2001]. Besides their climatic effects, light scattering and absorption by aerosols cause reduction in solar radiation [*Luria et al.*, 1996] and influence visual air quality, thereby adversely impacting visibility and the aesthetic quality of the atmosphere [*Ganor et al.*, 1991; *Stanhill and Moreshet*, 1992; *Ganor*, 1994; *Seinfeld and Pandis*, 1998].

[3] Atmospheric aerosols, of both natural and anthropogenic origin, can affect climate directly by scattering and absorbing solar radiation [*Charlson et al.*, 1992] and indirectly by their ability to nucleate cloud droplets [*Twomey*, 1977]. Assessment of the indirect effect requires measurements outside the scope of the present study and will not be addressed here. Depending on the optical properties of the aerosol, the sign, or direction of climate forcing, can be positive (warming) or negative (cooling). Anthropogenic aerosols and human perturbations in the fluxes of natural aerosols contribute to the direct effect. The major anthropogenic components are sulfate, biomass smoke, and black carbon from fossil fuel burning with estimated forcings of −0.4, −0.14 to −0.3, and +0.2 W m^{-2}, respectively [*Shine and Forster*, 1999, and references therein].

[4] A major natural component of atmospheric aerosol is mineral dust, which enters the atmosphere from dust storms in arid and semiarid regions. Changes in land use practices are thought to have increased the rate of dust emission, resulting in a climate forcing of +0.1 W m^{-2} [*Tegen et al.*, 1996] at the top of the atmosphere, with an arbitrarily assigned uncertainty of ±0.4 W m^{-2} [*Shine and Forster*, 1999]. At the local level, in

[1]Now at Science Systems and Applications Inc., Climate and Radiation Branch, NASA Goddard Space Flight Center, Greenbelt, Maryland, USA.

0148-0227/02/2001JD900252$09.00

areas with prevalent dust storms, dust can be the dominant aerosol component present and the forcing can vary, for example, from +5 to −3 W m^{-2} between Arabia and the Arabian Sea, as described by *Shine and Forster* [1999]. On the basis of their measurements of African mineral dust at Barbados, *Li et al.* [1996] found that throughout the tropical and subtropical North Atlantic region, mineral dust from Africa should be the dominant light-scattering aerosol. They proposed that mineral dust over this region, and other regions where anthropogenically enhanced dust concentrations are high, could be an important climate-forcing agent. Mineral dust has, however, only recently begun to be included in calculations of radiative forcing. The associated uncertainties are considerable, given the high variability of the dust loading in space and time, and our limited knowledge of dust optical properties in many regions of the Earth [*Claquin et al.*, 1998; *Tegen and Miller*, 1998; *Ginoux et al.*, 1999; *Sokolik and Toon*, 1999; *Guelle et al.*, 2000]. It is obvious from the preceding discussion that much more information is required on the spatiotemporal distribution and the size-dependent chemical and optical properties of atmospheric aerosols [*Andreae*, 1995; *Schwartz and Andreae*, 1996; *Penner et al.*, 2001].

[5] The aerosol mass-scattering efficiency (α; m^2 g^{-1}), which is also referred to as mass-scattering coefficient or specific light scattering, is determined using concurrent measurements of the aerosol light-scattering coefficient (σ_{sp}) and some estimate of particle mass [*Hegg et al.*, 1996; *Charlson et al.*, 1999]. Many previous derivations of α have been made using only sulfate to represent particle mass, and other components, such as mineral dust and carbonaceous aerosols, were not considered. Furthermore, earlier climate-modeling work also focused on sulfate aerosols as the presumably dominant anthropogenic light-scattering species [*Waggoner et al.*, 1976; *Charlson et al.*, 1991; *Kiehl and Briegleb*, 1993]. It is now clear, however, that this assumption is not valid and that aerosol species other than sulfate make important contributions to scattering [*Malm et al.*, 1994; *Andreae*, 1995; *Houghton et al.*, 1996; *Novakov et al.*, 1997; *Penner et al.*, 2001].

[6] To improve our knowledge of the radiative properties of atmospheric aerosols, their origin, and their spatiotemporal distribution, we have initiated in 1995 the Aerosol Radiation and Chemistry Experiment (ARACHNE) research program, a set of long-term measurements at selected locations in the eastern Mediterranean region. Model calculations show that global circulation patterns tend to transport pollutants, emitted from central and eastern Europe, toward the Mediterranean and the Middle East. Therefore high concentrations of pollution aerosols are expected in this region. Particularly, anthropogenic sulfate levels and their direct radiative effects are predicted to be very pronounced there [*Langner et al.*, 1992; *Chin and Jacob*, 1996; *Feichter et al.*, 1996]. Also, the region is subject to long-range transport of desert-dust aerosols from the deserts of North Africa and the Near East, with mineral dust being a major component of aerosol mass [*Levin and Lindberg*, 1979; *Ganor and Mamane*, 1982; *Ganor et al.*, 1991]. These factors and the frequent cloud-free conditions make the study area highly suitable to test our present understanding of the production and transport of aerosols and of their impact on the Earth's radiation budget.

[7] This paper is one in a series of publications resulting from the ARACHNE program (for details of other aspects of this program, and in particular the results of the winter and summer intensive campaigns, refer to *Ichoku et al.* [1999]and *Formenti et al.* [2001b], respectively). Here we will focus on the optical properties, mass-scattering efficiencies, and chemical composition of atmospheric aerosols measured at a field site at Sde Boker (30°51′34°47′E, 470 m above sea level (asl)), in the Negev desert, Israel. Using the data set we have collected at this site over a 2 year period, we present mass-scattering efficiencies obtained by a multivariate regression of the scattering coefficients on dust, sulfate, and residual components.

2. Methods

[8] Aerosol-scattering coefficients were measured with a three wavelength integrating nephelometer (TSI model 3563: TSI Incorporated, St. Paul, Minnesota, USA). This instrument makes continuous measurements of the atmospheric light-scattering coefficients for both total scattering and backscattering of in situ aerosols. Scattered light that passes through dichroic beam splitters and 40 nm bandpass filters centered at 450, 550, and 700 nm is detected by three photon-counting photomultiplier tubes (PMTs). Particle-scattering signals are both sensitive and stable over long periods of time because the instrument contains several noise and drift compensation features. The dark current of the detectors, variations in the light source intensity, and temperature, pressure, and humidity are continually measured. In addition, instrument wall scatter is periodically monitored by passing the inlet air through an in-line high-efficiency particulate air (HEPA) filter. These features make the nephelometer suitable for long-term field deployment.

[9] The nephelometer has one humidity and two temperature sensors. One temperature sensor is located at the sample inlet. Since the instrument was housed in a room without air conditioning, the temperature at the inlet was usually warmer than the outside ambient temperature. The other temperature sensor and the humidity sensor are located near the sample outlet, and it is these values that are used in the calculations as representing conditions inside the measurement chamber. For our instrument at Sde Boker the outlet temperature was always ∼3° C warmer than the inlet temperature, due to the heat produced by the nephelometer. Therefore the sample humidity measured near the sample outlet is always lower than ambient.

[10] For the duration of the measurement period, data were recorded around the clock at 2 min intervals. The inlet consisted of ∼ 5 m of 2.2 cm ID plastic hose that was fitted with a funnel covered by an insect screen. The inlets for the nephelometer and the stacked filter unit (SFU) sampler (described below), which both faced downward, were located adjacent to one another on a rooftop ∼ 4 m above ground. No attempt was made to limit the size range of the particles entering the instrument.

[11] The instrument was calibrated following the instructions of the manufacturer, using compressed air or filtered ambient air for the low span gas and CO_2 for the high span gas. A series of calibrations was conducted in the laboratory, and the instrument was calibrated when first placed in the field and then periodically during the 2 year data collection period. The calibration coefficients over the first year and a half of the study period showed coefficients of variation for the blue, green, and red wavelengths of 1.5, 0.34, and 3.9%, respectively. Between the field calibration of 21 June 1996 and the next field calibration of 9 March 1997, there was a change of 8% that was assumed to be linear over this time period, and a data correction was applied accordingly. For more detailed discussions of the performance characteristics of this instrument refer to *Anderson et al.* [1996], *Anderson and Ogren* [1998], *Caldow et al.* [1994], and *Bodhaine et al.*, [1991].

[12] Corrections were made to account for the truncation of near-forward scattered light and the non-Lambertian illumination intensity of the TSI 3563 [*Anderson and Ogren*, 1998]. To account for the particle-size dependence of the truncation error, we used the correction equations based on the observed Ångström coefficients, as proposed by *Anderson and Ogren* [1998]. For the submicron aerosol, these corrections are minor (<10%), while for the coarse mineral dust aerosol, they may reach ∼50%. The near-forward truncation error is of minor importance for the climatic effect of the aerosol, however, since the light scattered in the near-forward direction will also reach the Earth's surface and not be scattered

Table 1. Temperature and Humidity Statistics for Sde Boker, January 1996 to December 1997

Month	Temperature, °C			Relative Humidity, %		
	Average	Minimum	Maximum	Average	Minimum	Maximum
Jan. 96	9.8	−0.7	20.2	75.9	16.0	99.8
Feb. 96	11.8	0.7	20.2	65.3	8.2	99.6
March 96	12.9	1.9	29.0	63.8	17.5	100.0
April 96	16.4	4.9	35.4	58.5	8.4	99.2
May 96	21.9	9.0	40.1	53.5	7.7	100.0
June 96	23.1	13.3	36.0	57.9	12.0	99.4
July 96	25.6	15.7	37.6	60.2	12.4	100.0
Aug. 96	25.1	13.7	36.7	63.2	17.9	99.0
Sept. 96	23.6	11.9	39.0	63.2	10.7	98.7
Oct. 96	19.1	6.4	32.5	64.3	14.5	98.1
Nov. 96	16.1	4.8	26.2	66.6	16.5	99.7
Dec. 96	11.9	1.3	24.6	67.8	9.9	100.0
Jan. 97	9.8	1.1	23.4	73.9	9.0	99.9
Feb. 97	7.9	−2.6	22.7	70.9	26.9	100.0
March 97	10.8	−0.3	26.2	67.7	14.0	96.9
April 97	15.2	−0.4	37.7	54.9	9.0	100.0
May 97	21.4	6.9	33.9	50.1	8.9	98.1
June 97	23.7	9.9	39.6	55.6	11.3	100.0
July 97	25.2	14.6	36.7	57.1	14.6	99.5
Aug. 97	23.8	14.2	35.7	64.7	18.0	100.0
Sept. 97	22.2	12.1	32.1	66.3	21.3	99.2
Oct. 97	20.3	8.1	35.2	64.6	17.3	98.7
Nov. 97	15.5	6.1	25.3	68.5	22.0	100.0
Dec. 97	11.1	0.6	20.7	74.6	26.6	100.0

back into space except at very large zenith angles. To allow comparison with other work, both corrected and uncorrected values will be reported. Scattering by particles (σ_{sp}) is given in units of inverse megameter (Mm^{-1}).

[13] Aerosol sampling at Sde Boker was begun in January 1995 and continues to this day. The complete aerosol data set will be referred to in this paper as the "long-term" data set, while the subset chosen for presentation in this paper (obtained during December 1995 to October 1997, the time that the nephelometer was in operation) is referred to as "this study." Each week, two 2 day and one 3 day samples were taken using the "Gent" PM10 stacked filter unit (SFU) sampler. The "Gent" sampler operates at an airflow rate of 15–16 L/min and works according to the same principles as other SFU variants [*Heidam*, 1981; *John et al.*, 1983; *Cahill et al.*, 1990]. It utilizes two 47 mm diameter Nuclepore polycarbonate filters, with pore sizes of 8 μm (Apiezon vacuum grease coated) and 0.4 μm, which are placed in series. The 50% cutoff diameter for the 8 μm filter, at the face velocity used, is ~2 μm. Upstream of the coarse filter is a preimpaction stage that has a calculated 50% cutoff diameter of 10 μm and thus acts as a PM10 (particulate matter 10 μm) inlet. The impaction plate of the preimpaction stage is coated with Apiezon vacuum grease in order to reduce particle bounce-off. Consequently, the coarse Nuclepore filter collects the 2–10 μm equivalent aerodynamic diameter (EAD) size fraction, whereas the fine filter collects the particles <2 μm EAD. The air was drawn through the sampler with a diaphragm vacuum pump. The air volume is measured with a calibrated dry gas meter. Air volumes at ambient T and P are used for calculating concentration data.

[14] The coarse and fine filters from the SFU samples were analyzed for coarse and fine particulate masses (CPM and FPM) by gravimetry, for black carbon equivalent (BCE) (the concentration of black carbon corresponding to a measured light extinction at fixed absorption efficiency) by light reflectance, for soluble ionic species by ion chromatography (IC) and capillary zone electrophoresis (CZE); and for up to 48 elements (from Na to Th) using a combination of instrumental neutron activation analysis (INAA) and particle-induced X-ray emission analysis (PIXE). The IC and CZE analyses were limited to the samples from the two intensive campaigns and a few long-term samples from 1995. The gravimetric analysis was done by weighing each filter before and after sampling with a microbalance (1 μg sensitivity) in a room with stabilized temperature (20°C) and relative humidity (50%). The filters were preequilibrated in this room for at least 24 hours, and during the actual weighing, static electricity was eliminated from the filter by means of a ^{210}Po radioactive source. The BCE analysis is based on a light reflectance technique [*Andreae*, 1983; *Andreae et al.*, 1984] performed with a commercial smoke stain reflectometer (Diffusion Systems Ltd., London, England, UK, model 43). To dissolve the ionic species for IC or CZE analysis, the Nuclepore filters are cut up, placed into polyethylene or polystyrene bottles, and extracted with deionized water. The anions measured are nitrite, nitrate, sulfate, chloride, and bromide. The cations measured are Na^+, NH_4^+, K^+, Mg^{2+}, and Ca^{2+}. The IC method is described in detail by *Maenhaut* [1997]. The CZE analyses were carried out according to *Beck and Engelhardt* [1992]. The following elements were measured by INAA using one half of each filter: Na, Mg, Al, Cl, K, Ca, Sc, Ti, V, Cr, Mn, Fe, Co, Ni, Cu, Zn, Ga, As, Se, Br, Rb, Sr, Mo, Ag, Cd, In, Sn, Sb, I, Cs, Ba, La, Ce, Sm, Eu, Lu, W, Au, and Th. The neutron irradiations, gamma spectrometric counting, and quantification methods were similar to those described by *Maenhaut and Zoller* [1977] and *Schutyser et al.* [1978]. A quarter section of each filter was used for PIXE, and the following elements were measured: Na, Mg, Al, Si, P, S, Cl, K, Ca, Ti, V, Cr, Mn, Fe, Ni, Cu, Zn, Ga, Ge, As, Se, Br, Rb, Sr, Y, Zr, Nb, Mo, Ba, Pb, U, and Th. The experimental setup and analytical procedures used in these PIXE analyses have been presented before [*Maenhaut et al.*, 1981; *Maenhaut and Raemdonck*, 1984]. For further detailed descriptions of the "Gent" SFU sampler and chemical analysis techniques refer to *Maenhaut et al.* [1996a] and *Maenhaut* [1997].

3. Results and Discussion

3.1. Study Site Description and Climatology

[15] All measurements were made in Sde Boker (30° 51′N, 34° 47′E, 470 m asl), Israel, at the site of the Jacob Blaustein Institute for Desert Research, of the Ben Gurion University of the Negev. Sde Boker, about 100 km inland from the eastern Mediterranean

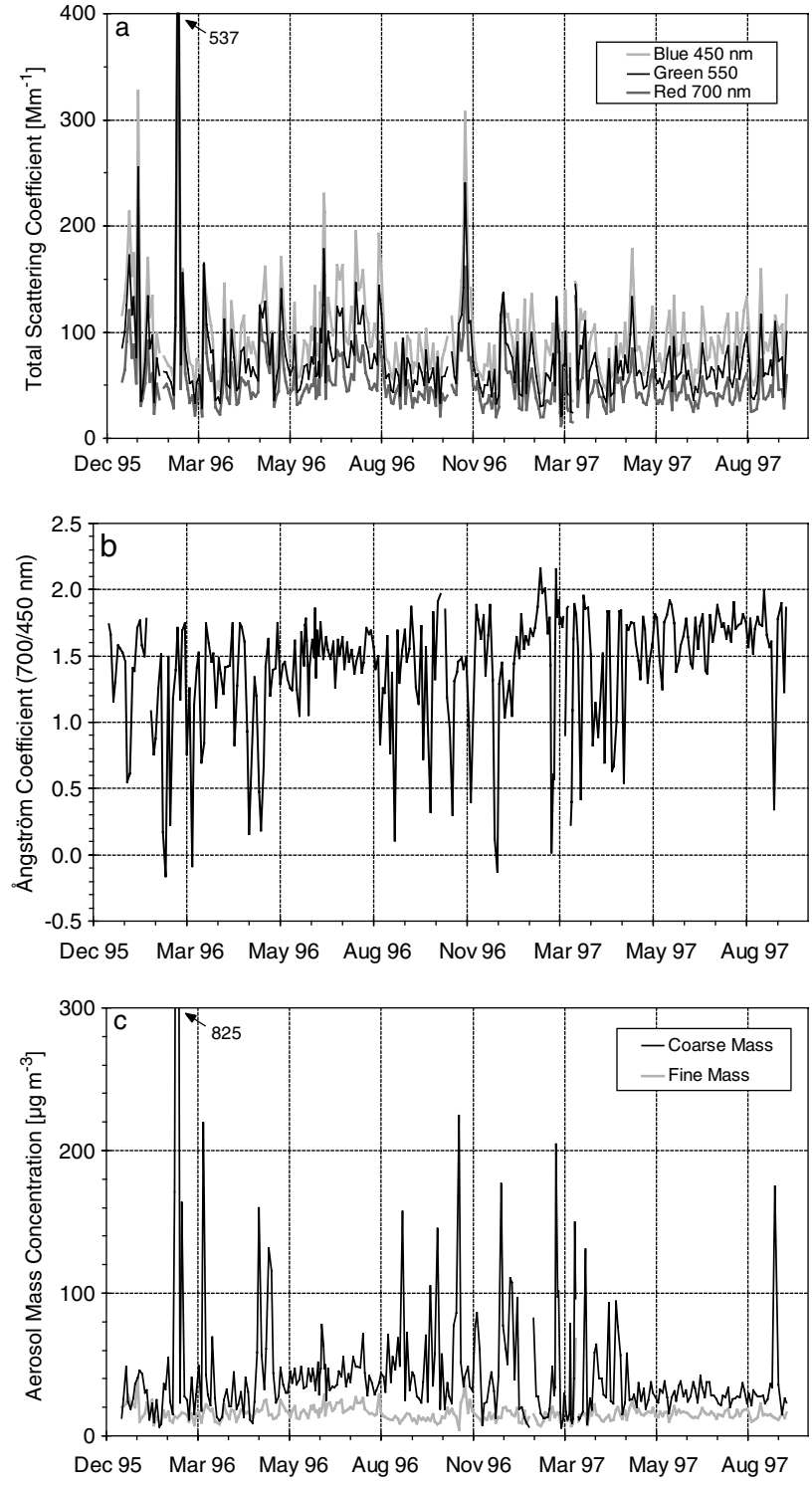

Figure 1. Time series plot of (a) total scattering for three wavelengths, (b) Ångström coefficient, (c) coarse and fine aerosol mass, and (d) calculated anthropogenic and dust total scattering.

Sea is in the northern part of the Negev desert, at the southern boundary of the Israeli transition belt, a 50 km wide zone with a steep climatic gradient. Mean annual rainfall decreases from 200 to 100 mm over this transition belt. The annual rainfall at Sde Boker, occurring all in winter is about 100 mm. Temperature and humidity statistics for Sde Boker are compiled in Table 1. The coldest and most humid months of the year are January and February, the hottest months are July and August, and the driest month is May.

[16] In a study of dust events over Israel covering the 33 year period of 1958–1991, *Ganor* [1994] shows that the dusty season begins in October. The frequency of dust episodes remains steady through February, then approximately doubles during the period of April through May, after which it drops sharply. July and August are nearly dust free. Large amounts of dust originating in the Saharan belt (Chad, Libya, Egypt, and Saudi Arabia) are blown over the Mediterranean and reach Israel (estimated 70×10^6 tons per year)

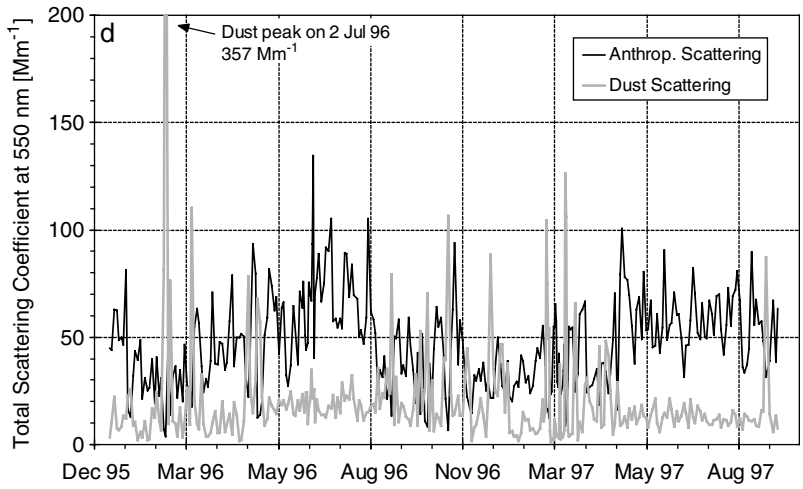

Figure 2. (continued)

with approximately one third of this total settling over the country [*Ganor*, 1994]. Airflow over the east Mediterranean is generally from west to east. Air mass back trajectories, studied over a 5 year period at the 850 hPa level, show that 36% of the time, air masses reaching Israel have originated from northwestern Europe and 30% of the time from northeastern Europe [*Dayan*, 1986].

3.2. Scattering Coefficients, Time Series, and Ångström Coefficient

[17] Total scattering as recorded by the three wavelength nephelometer for the study period of 14 December 1995 until 9 October 1997 (this study) is shown in Figure 1a, and a statistical summary of the scattering data is presented in Table 2. The data represent averages for the same 2–3 day periods over which the aerosol samples were collected. To eliminate the influence of the sharp nonlinear increase in σ_{sp} at high humidities that sometimes occur in the early morning hours, data with RH>80% in the instrument chamber have been removed from the data set.

[18] The total mass scattering coefficients at 450 nm (blue), 550 nm (green), and 700 nm (red) vary from low values of ~ 20 Mm^{-1} to a highest value of $\sim$ 500 Mm^{-1}. The (uncorrected) total scattering coefficient at 550 nm showed a median of 66.7 Mm^{-1} (mean and standard deviation: 75.2 ± 41.7 Mm^{-1}) typical of moderately polluted continental air masses. For comparison, scattering coefficients of 26 Mm^{-1} for a clear day and 410 Mm^{-1} for a day with heavy smog have been reported for Los Angeles, California, USA [*Seinfeld and Pandis*, 1998]. *Hegg et al.* [1997] reported values ranging from 20 to 195 Mm^{-1} off the mid-Atlantic coast of the United States, *ten Brink et al.* [1996] reported an annual average of 71 Mm^{-1} and values as low as 5 Mm^{-1} (for marine arctic air) measured in the Netherlands, and values ranging from 3.7 to 155 Mm^{-1} were reported for Barbados [*Pilinis and Li*, 1998]. Comparison of the instrument-error corrected and uncorrected values shows significant differences.

[19] The Ångström coefficient å, which represents the wavelength dependence of scattering (σ_{sp}) was calculated according to the following formula:

$$\text{å} = \ln(\sigma_{sp\,700}/\sigma_{sp\,450}) / \ln(\lambda_{700\text{nm}}/\lambda_{450\text{nm}})$$

[20] The Ångström coefficient increases with decreasing particle size. For aerosol particles with a volume mean diameter of ≈1.5 μm and larger (coarse) particles, the Ångström coefficient is zero or slightly negative, and for particles of less than 1μm diameter (fine), it is 1 or greater [*Seinfeld and Pandis*, 1998]. In our data set, it ranged from −0.16 to 2.16, with an average ± standard deviation and a median value of 1.41 ± 0.44, and 1.52 for the uncorrected data and 1.43 ± 0.41 and 1.53 for the instrument-error corrected data (Figure 1b and Table 2). Because of the ratioing process that goes into the calculation of the Ångström coefficient, the effect of the correction nearly cancels out the effect of using either the corrected or the noncorrected data. The lowest values were found during dust events. In our results, there is a clear relationship between the Ångström coefficient and the relative abundance of coarse and fine aerosols as measured by the ratio

Table 2. Scattering Coefficients (σ_{sp}), Ångström Coefficient (*å*), and Backscatter Ratios (*b*) Obtained During the Study Period at Sde Boker[a]

Property	450 nm	550 nm	700 nm
σ_{sp}	96.5 ± 45.3	75.2 ± 41.7	53.7 ± 37.7
	88.8	*67.7*	*45.8*
σ_{sp} (corrected)	110.8 ± 56.5	86.7 ± 53.8	62.0 ± 48.7
	99.2	*75.4*	*51.6*
$\mathring{a}_{(700\text{nm}/450\text{nm})}$	...	1.41 ± 0.45	...
		1.52	
$\mathring{a}_{(700\text{nm}/450\text{nm})}$ (corrected)	...	1.43 ± 0.41	...
		1.53	
b	0.12 ± 0.02	0.13 ± 0.02	0.16 ± 0.02
b (corrected)	0.10 ± 0.01	0.12 ± 0.02	0.14 ± 0.02

[a] For σ_{sp} and *b*, values with and without corrections for the instrument artefacts of the TSI 3563 are presented. Means and standard deviations are given for all parameters; since σ_{sp} and *å* are influenced by a relatively small number of high values from dust episodes; the median is also shown for these parameters (in italics).

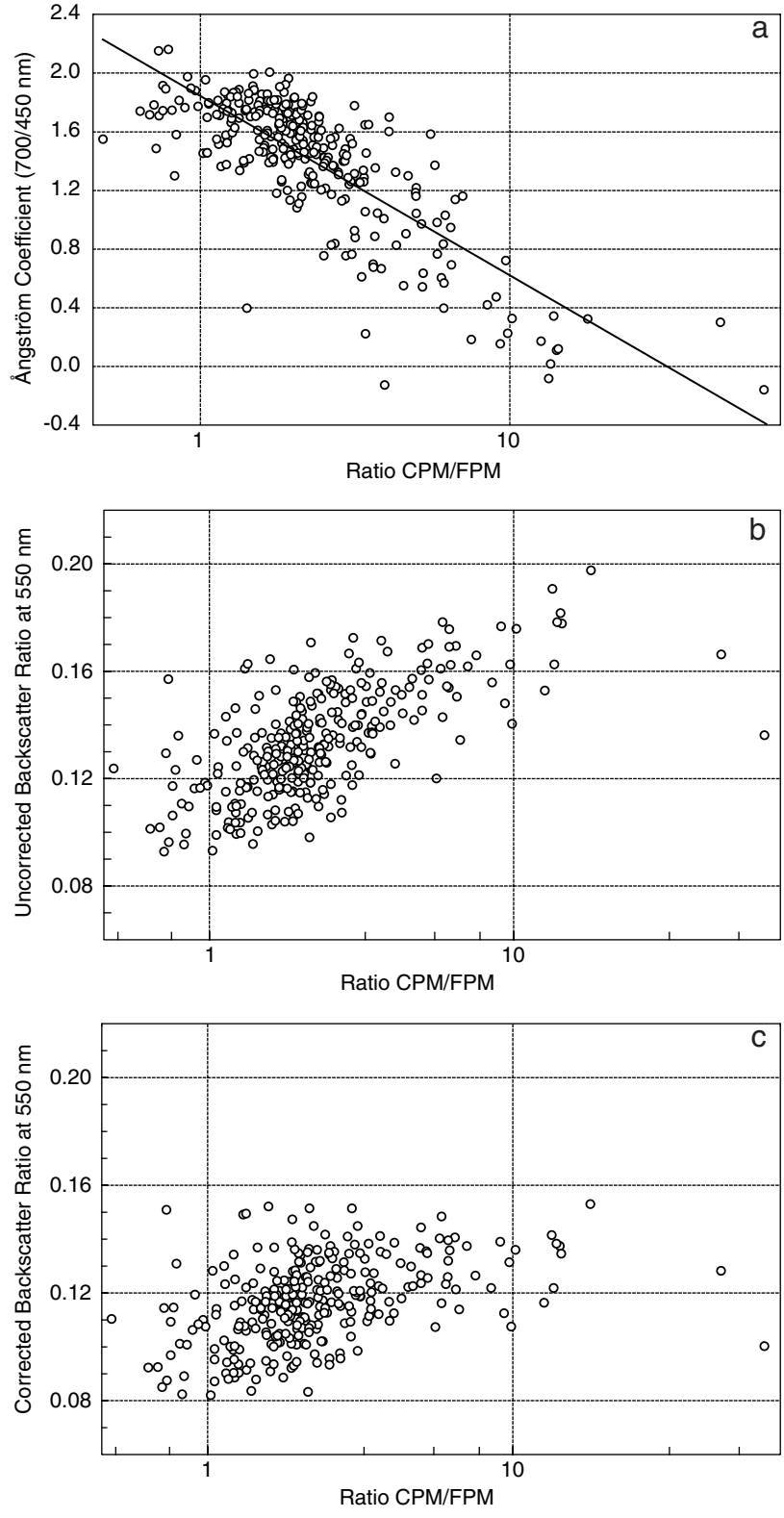

Figure 2. Scatterplot of the ratio of coarse particulate mass (CPM) to fine particulate mass (FPM) against (a) the Ångström coefficient, (b) the uncorrected backscatter ratio (550 nm), and (c) corrected backscatter ratio (550 nm).

CPM/FPM (Figure 2a). The Ångström coefficient declines with an approximately logarithmic dependence from values around 2 for samples dominated by fine aerosol to values around zero during dust storms, in good agreement with the behavior expected from Mie theory [*Seinfeld and Pandis*, 1998].

[21] The backscatter ratio at Sde Boker falls within a narrow range (0.13 ± 0.02) and is close to values from polluted air masses reported from other regions, for example, 0.14 ± 0.02 from continental air masses in the northwestern and eastern United States [*Anderson et al.*, 1999; *Sheridan and Ogren*, 1999]. A plot

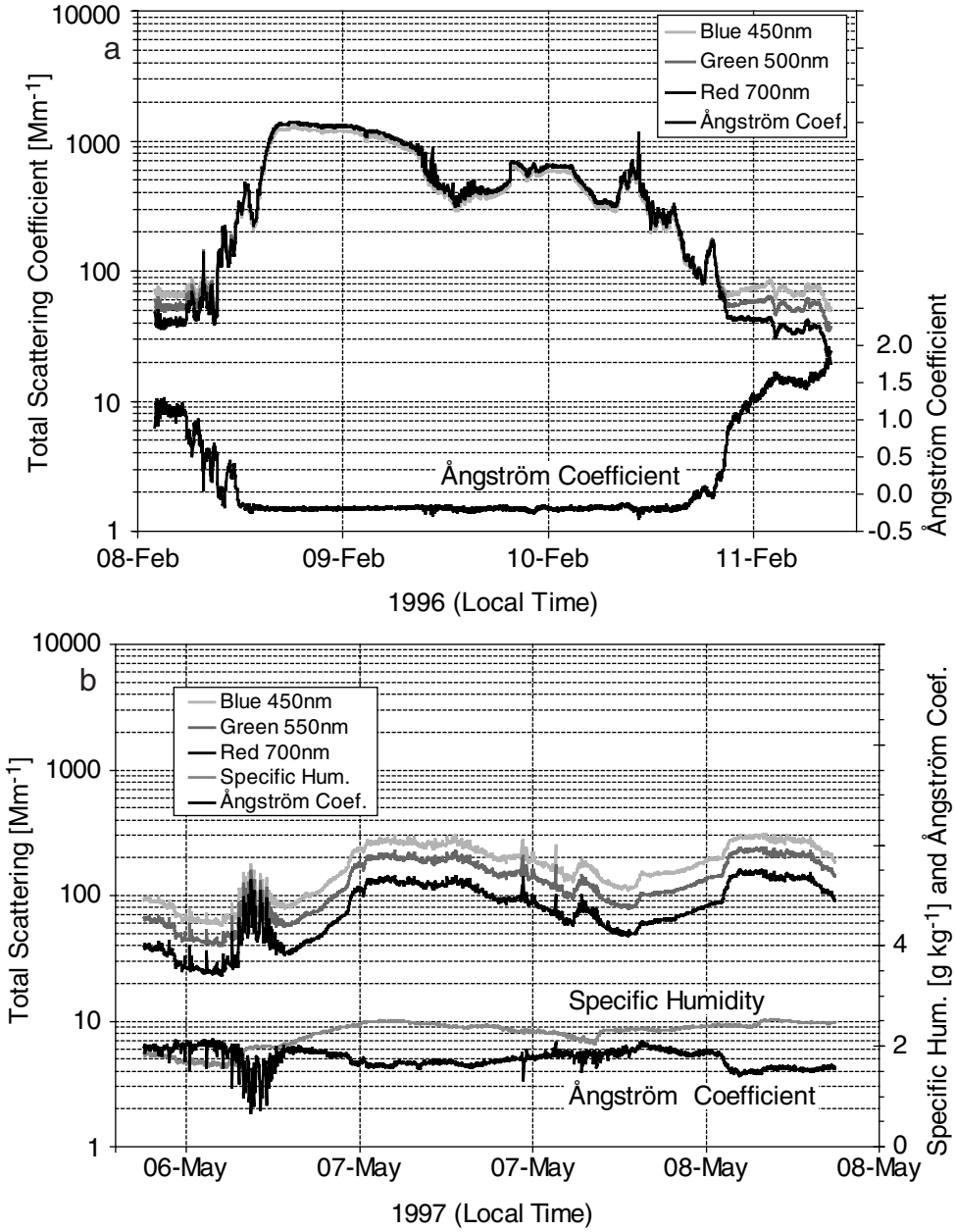

Figure 3. Time series plot showing the total scattering at three wavelengths and the Ångström coefficient for (a) the case study of 8–11 February 1996 and (b) the case study of 6–8 May 1997.

of the backscatter ratio (i.e., the ratio of scattering in the backward hemisphere to total scattering) versus CPM/FPM shows an apparent increase of this ratio with increasing relative abundance of coarse aerosol (Figure 2b). This is in conflict with theoretical expectations, which would predict that the fraction of backscattered light decreases with particle size. The observed positive correlation appears to be an artefact of the nephelometer geometry. When the backscatter ratio is calculated using the instrument-error corrected values of total scattering, there is no significant relationship between this ratio and the CPM/FPM (Figure 2c). The lack of the expected negative correlation between backscatter ratio and size may be due to a residual instrumental artefact or to the relatively weak size dependence of the two parameters for particle sizes larger than 0.7 μm diameter [*Nemesure et al.*, 1995]. It may also be related to the difficulties associated with the application of Mie theory to large, nonspherical particles (T. L. Anderson, personal communication, 2000).

[22] To identify dust events in our data set, we used the following criteria: (1) the total scattering coefficient at 550 nm must be at least 150 Mm^{-1} for at least 1 hour and (2) Ångström coefficients must be less than 0.92 (outside of dust events, this value is normally greater than 1.4). During the study period, 31 such dust events were detected, which were characterized by a sharp drop in the Ångström coefficient to values near zero. During the most severe dust storm events, we recorded 2 min average values of 1000 Mm^{-1} and higher. As discussed in section 3.1, the months with the fewest dust events are July and August. In 1996 we recorded one dust event on July 18 and one on August 12, and in 1997, we had no recorded dust events in either of these months. During the rest of the year no obvious seasonal pattern is evident. During the measurement period, we collaborated with project MEDUSE (Mediterranean Dust Experiment) in which dust events for the Mediterranean area were predicted using models. We participated in verifying, through our field observations and

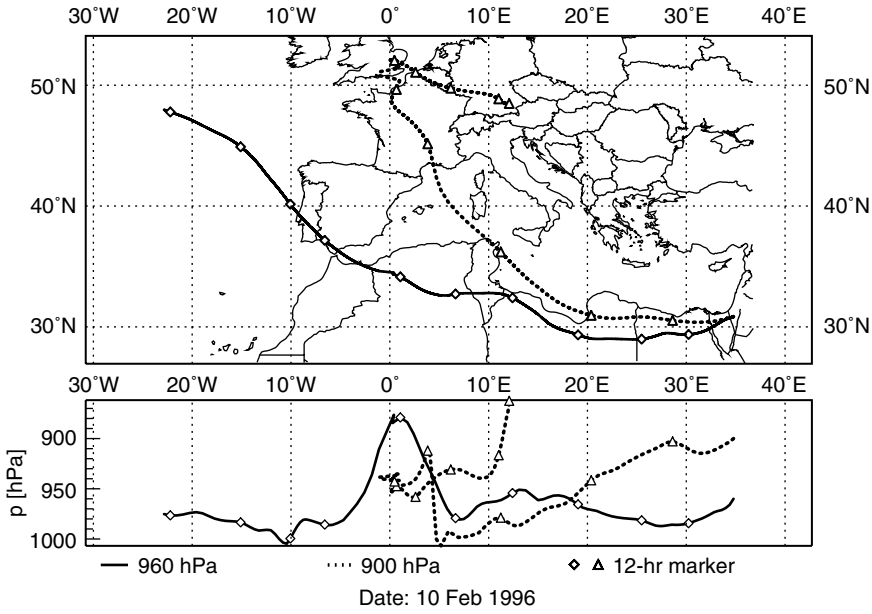

Figure 4. Five day air mass back trajectories at 960 and 900 hPa arriving at Sde Boker on 10 February 1996. The bottom panel shows the altitude (pressure level) of the air mass along the trajectories.

measurements, the timing and intensity of dust events predicted for the Sde Boker area. The results of this work are available on the Internet, web site http://www.halo.is/meduse/.

[23] To illustrate in more detail the physical and chemical properties of the aerosol at Sde Boker, we have selected days in February 1996 and in May 1997 which represent dusty and polluted conditions, respectively. In Figures 3a and b we show the total scattering and the Ångström coefficients determined at 2 min intervals for these periods, in Figures 4 and 5 the back trajectory analyses to determine the origin of sampled air masses, and in Table 3 the chemical composition of the aerosol. These trajectories are representative cases for a complete set of trajectories that we have compiled for our site.

[24] For the time period of 8–12 February 1996, total scattering for all three wavelengths is shown in Figure 3a. During this period, a dust event lasting about 2 days occurred. The scattering values in the morning of 8 February are moderate, centering at 50 Mm^{-1} at midmorning. The Ångström coefficient has a value of about 1.3 during this period. By late afternoon, the onset of the dust event is evident as the scattering begins to rise and the spectral dispersion of the scattering diminishes, shown by a drop in the Ångström coefficient. By midnight, scattering increases to 1000 $Mm^{-1}$and remains elevated at about 500 Mm^{-1}. During the night of 11 February the scattering returns to about 50 $Mm^{-1}$and the scattering at the three different wavelengths becomes again clearly separated as the dust event ends at midday.

[25] During the entire dust event, the Ångström coefficient remained constant at a value of about −0.2, confirming that the scattering is due to coarse particles that consist, for our study region, mostly of $CaCO_3$ and silicate dust [*Ganor and Mamane*, 1982], with sea salt making up only a minor fraction of the aerosol mass (Table 3). The analysis of the chemical composition of the filter samples for these days shows that values in the coarse fraction for Al, Si, Ca, and Fe, the elements typically considered as dust tracers, are elevated by factors of 10–30 compared to the average values for the long term and for this study (Table 3). Na and Cl are also elevated in the coarse fraction, indicating a marine component of the air mass. In contrast, the species indicating pollution, i.e., fine sulfur and lead, are much below the long-term average and approach background levels.

[26] Five-day back trajectory analysis (Figure 4) shows that air masses reaching Sde Boker at 960 hPa on 9 and 10 February, the dusty days, originated over northern Libya and Egypt. This is consistent with the findings of *Dayan* [1986] that elevated concentrations of suspended particulates are observed in Israel in winter and spring when synoptic conditions bring air up from North Africa. Some of the low-level trajectories for this period (8–11 February 1996) show a passage of the air masses over the Red Sea or the Mediterranean, which could explain the presence of the sea-salt aerosol component.

[27] Figure 3b shows total scattering for all three wavelengths and the Ångström coefficient for 6–8 May 1997, a time of low dust levels and high amounts of pollution as is seen by the elevated levels in the fine fraction of the combustion indicators, BCE, V, Pb, and S, compared to the averages for this study and long term (Table 3). The scattering values range from about 50 to 200 Mm^{-1} during this period. The scattering time series shows a combination of local and long-range effects frequently observed at the Sde Boker site. On 6 May and, to a lesser extent, on 7 May, scattering is seen to rise for a few hours in the afternoon and then return to the values of midmorning. Such episodes of elevated scattering are often very spiky (as for 6 May) and are caused by local dust re-suspension, or thermal dust devils, which often occur in the desert during the afternoon [*Formenti et al.*, 2001a]. The occurrence of dust devils on 6 May coincides with sharp drops in the Ångström coefficient, indicating coarse aerosol, while å averaged 1.75 during the rest of the time, confirming the presence of polluted air.

[28] After sunset the scattering values begin to rise (for 7 and 8 May, reaching about 200 Mm^{-1}) until sunrise when values begin to decline again. The relative humidity follows the same cycle, ranging from about 20% at about 1600 UT to about 55% at about 0000 UT on both days. Despite this coincidence, the change in scattering cannot solely be explained by humidity-controlled growth of the aerosol, which could only account for an increase of about 20–30% over this humidity range rather than the observed quadrupling. Two further factors contribute to the increase in aerosol loading, the diel cycle of convection-driven dilution of the planetary boundary layer (PBL) and a probable change in air

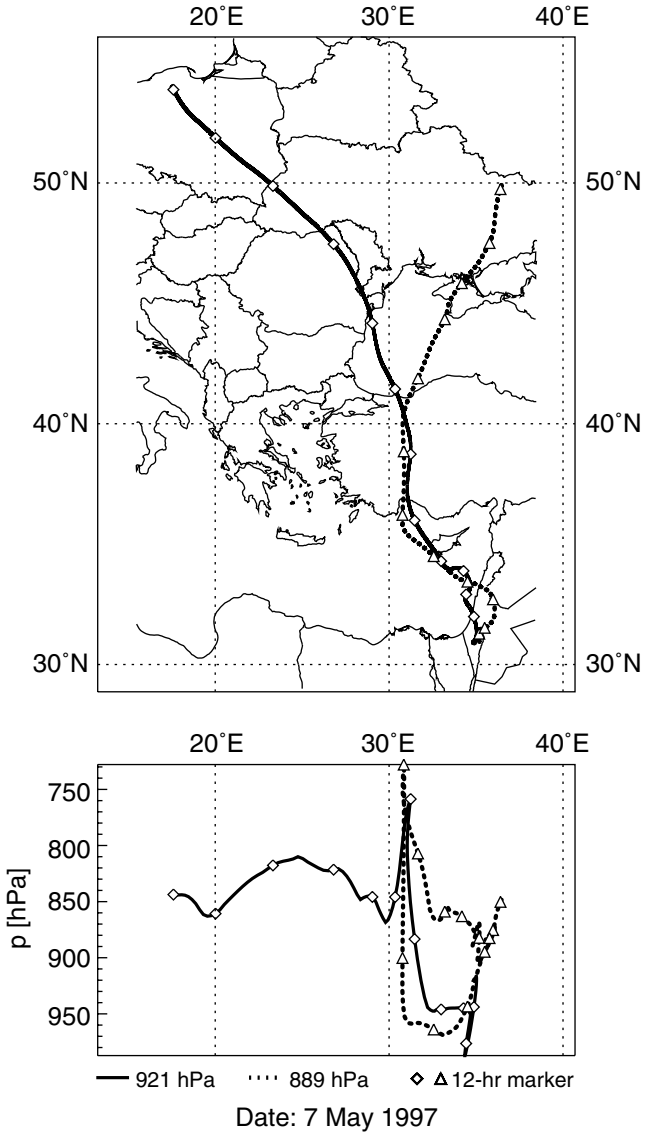

Figure 5. Five day air mass back trajectories at 960 and 900 hPa arriving at Sde Boker on 7 May 1997. The bottom panel shows the altitude (pressure level) of the air mass along the trajectories.

mass origin suggested by a sharp rise in specific humidity in the afternoon of 6 May.

[29] The commonly seen daytime decrease in scattering and aerosol loading at Sde Boker is related to both the diel cycle of relative humidity and the convective dilution of the pollution by growth of the PBL. The polluted air masses (the origins of which are discussed below) typically travel as layers of 1–3 km height below a relatively clean and dry free troposphere [*Formenti et al.*, 2001a]. Intensive convection over the desert leads to entrainment of free tropospheric air into the PBL and a reduction both of pollution levels and of the relative and specific humidity.

[30] Back trajectory analysis (Figure 5) shows that during the period 6–8 May near-surface air masses ($> \sim 900$ hPa) come from central Anatolia and across the Black Sea from Bulgaria, Romania, Ukraine, and Poland. At levels just above this layer, air mass trajectories come from the heavily industrialized Donets region of Ukraine. Emission inventories show these regions to be prolific sources of SO_2 (e.g., the IGAC/GEIA inventory available on the Internet at http://www.onesky.umich.edu/geia/emits/so2.html). We find that air masses originating in these countries, as well as in Germany, the Balkans, and Greece, are generally associated with high levels of pollution aerosol measured at Sde Boker. This was already noted by *Dayan* [1986] who found that trajectories originating in western, central, and eastern Europe and in Ukraine account for some 60% of trajectories reaching Israel on an annual basis and that these air mass origins are associated with polluted air.

3.3. Chemical Composition and Concentrations of Fine and Coarse Mode Aerosol

[31] The concentration for all chemical species measured in the fine and coarse mode aerosol for this study (14 December 1995 to 9 October 1997) are shown in Table 3. Also shown, for comparison, are the results for the long-term data set from 23 January 1995 to 26 November 1998. It is noteworthy that average values from the period analyzed in this study differ only in the minutest way from the complete 4 year long-term data set and can therefore be considered representative of the conditions at Sde Boker.

[32] Values for Al and SO_4^{2-} obtained at two sites in the eastern Mediterranean on the Turkish coast agree favorably with those from our site (taking into consideration differences in sampling and analysis and incident dustiness). At the Antalya site (30.34° E, 36.47° N), *Güllü et al.* [1998] report a geometric mean for SO_4^{2-} of 4250 ng m^{-3} and for Al of 300 ng m^{-3}. At the Erdemli site (36° 33′54″N, 34°15′18″E) in southeastern Turkey, *Kubilay and Saydam* [1995] report a geometric mean for Al of 685 ng m^{-3}. Our values for the Sde Boker site for this study (geometric means and in units of ng m^{-3}) are 7060 and 1694 for fine and coarse sulfate and 170 and 1044 for fine and coarse Al. Our results for sulfate are also in excellent agreement with the measurements at several sites in Israel by *Luria et al.* [1996], who found a mean of 9600 ng $SO_4^{2-}m^{-3}$ in samples collected without size discrimination, and at a site 40 km northwest of Damascus, Syria, where *Cornille et al.* [1990] found 5310 and 2100 ng m^{-3} for fine and coarse sulfate, respectively.

[33] The abundance of the major constituents of the fine and coarse mode aerosol is shown in Figure 6. The largest fraction in the fine mode is sulfate, the second largest fraction is carbonaceous aerosol, and the rest is accounted for by silicate and carbonate dust, nitrate, and sea salt. Sulfate mass was calculated as $(NH_4)_{1.86}H_{0.14}SO_4$, based on an observed ammonium to sulfate ratio of 1.86, and nitrate was assumed to be NH_4NO_3. The concentrations of organic and elemental carbon aerosol were estimated from the measurements of BCE done year-round on the SFU samples, and thermo-optical evolved-gas determinations of organic carbon (OC) and elemental carbon (EC) done during an intensive campaign at Sde Boker [*Ichoku et al.*, 1999]. The BCE measurement strongly overestimates the EC concentration, probably because of errors related to the internal mixing state of the aerosol [*Fuller et al.*, 1999], but the measurements are highly correlated. We therefore applied the EC/BCE slope obtained during the intensive campaign to the entire data set. Since OC data were also only available from the intensive campaign, we had to assume a constant OC/EC ratio (5.6, based on the data from the ARACHNE-97 campaign) throughout the year as well and to use this ratio to obtain an estimate of the annual mean OC concentration. Finally, the concentration of particulate organic matter was determined by multiplying the OC concentration with 1.4, the assumed average ratio of the mass of carbon-containing species to carbon mass. This value is based on the speciation of aerosol carbon mass sampled in highly polluted urban environments [*Groblicki et al.*, 1981; *Gray et al.*, 1986; *White*, 1990; *Hegg et al.*, 1997]. Silicate and carbonate dust were derived from Al and Ca, and sea salt from Na, as explained in more detail below when dealing with the coarse size fraction. The sum of the fine fraction aerosol components (15.0 μg m^{-3}) agrees very well with the mean fine fraction mass determined gravimetrically (15.1 μg m^{-3}), providing excellent mass closure on the fine aerosol.

Table 3. Comparison of Mass Concentrations of Chemical Species for Fine and Coarse Size Fractions Over Different Time Periods (Arithmetic Means and Standard Deviations)[a]

Size Class	Chemical Species	This Study 14 Dec. 95 9 Oct. 97		Long Term 23 Jan. 95 26 Nov. 98		Case Study 8 Feb. 96 11 Feb. 96		Case Study 6 May 97 8 May 97	
		Mass, ng m^{-3}		Mass, ng m^{-3}		Mass, ng m^{-3}		Mass, ng m^{-3}	
		Mean	SD	Mean	SD	Mean	SD	Mean	SD
Fine	PM, μg m^{-3}	15.9	5.9	15.8	5.7	13.0	0.6	22.5	2.1
	BCE	1232	508	1243	517	205	220	1637	302
	Na	199	109	199	109	60.8	2.3	198	9.2
	Mg	137	63	136	62	214	33	103	31
	Al	231	179	227	183	772	10	108	2.1
	Si	576	425	560	433	2152	5	261	4
	P	93	136	91	131	21	2	...	...
	S	1969	889	2003	933	164	5	4251	9
	Cl	62	62	58	56	51	9	109	12
	K	140	62	145	69	172	1	104	2
	Ca	807	584	765	605	1503	34	450	28
	Ti	15.9	11.7	15.8	12.1	54.6	0.5	8.1	0.4
	V	4.5	2.5	4.8	2.6	1.5	0.1	9.2	0.1
	Mn	4.1	2.2	4.2	2.3	9.1	0.3	6.8	0.2
	Fe	165	107	163	109	470	9	135	9
	Ni	2.4	1.7	2.5	1.7	0.7	0.2	3.9	0.2
	Cu	1.3	0.5	1.3	0.8	1.0	0.1	1.4	0.2
	Zn	15.5	16.5	17.3	25.9	3.7	0.3	118.2	1.6
	Br	16.7	16.1	16.5	14.9	1.2	0.7	11.2	1.2
	Sr	3.1	2.4	3.0	2.4	7.2	0.6	...	...
	I	2.1	0.7	2.2	0.8	0.5	0.1	2.3	0.1
	Pb	11.8	8.3	13.0	9.2	2.5	0.4	19.8	0.9
	Th	0.06	0.02	0.06	0.02	0.12	0.01	...	...
Coarse	PM, μg m^{-3}	44.5	56.5	42.9	58.8	498	327	27.3	1.4
	BCE	453	278	463	273	1430	215	315	310
	Na	1017	595	988	622	5000	220	675	16
	Mg	821	1044	783	1022	14190	1732	450	67
	Al	1722	3221	1640	3135	47160	1416	762	15
	Si	3358	4967	3226	4991	66180	110	1478	8
	P	255	464	248	447	466	23	56.9	3.7
	S	677	476	664	484	3433	26	667	5
	Cl	1137	891	1069	899	5700	186	318	34
	K	459	636	444	627	9003	37	212	2
	Ca	5937	6208	5773	7065	58360	1914	3237	96
	Ti	110	18	107	188	2700	17	50.6	0.9
	V	5.3	6.2	5.1	6.2	72.1	5.4	3.7	0.1
	Mn	20.8	31.8	20.0	30.7	438	25	11.4	0.7
	Fe	1128	2014	1082	1999	29560	2104	575	57
	Ni	3.3	3.7	3.2	3.3	31.6	3.5	1.9	0.3
	Cu	2.8	2.0	2.7	2.2	15.5	3.6	2.4	0.2
	Zn	15.1	14.4	15.2	13.6	98	5	38.9	0.6
	Br	12.5	13.9	12.0	14.3	...	...	9.8	2.7
	Sr	20.7	28.2	20.5	31.7	342	17	6.7	0.9
	I	1.4	1.4	1.4	1.4	14.6	3.2	0.70	0.11
	Pb	8.2	7.4	8.3	7.6	68.5	9.3	8.5	0.8
	Th	0.25	0.53	0.24	0.48	8.1	0.1	0.10	0.02

[a] PM is particle mass in μg m^{-3}. Values below the detection limit are indicated by three center dots.

[34] Our data suggest that the fine mode aerosol is composed predominantly of anthropogenic components. The sulfate, nitrate, and carbonaceous aerosol components together make up ~75% of this size fraction. Since the observed sulfate concentrations are at least an order of magnitude above what could be expected from natural sources in this region [*Herut et al.*, 1995; *Chin and Jacob*, 1996] and since there is little natural carbonaceous or nitrate aerosol expected to be present in this arid environment, we propose that essentially all of these components are of anthropogenic origin.

[35] Our observations of the coincidence of trajectories arriving from Europe, Russia, and Ukraine with high loadings of these anthropogenic aerosols suggest long-range transport as the dominant aerosol source for the Israel region. Given the high population density in Israel, and the presence of large power plants along the coast, one would expect that sources in Israel and the other Near East countries contribute to the aerosol loading in the study region. There is, however, a considerable body of evidence that suggests that long-range transport dominates the pollution aerosol budget, particularly for the optically most active accumulation mode [*Luria et al.*, 1996; *Ichoku et al.*, 1999; *Formenti et al.*, 2001a, 2001b]. In the dry climate of the Near East region, SO_2 from regional sources is to a large extent advected out of the region before it can be converted to sulfate aerosol. Further support for the predominance of anthropogenic sulfate from distant sources comes from the uniform isotopic composition ($\delta^{34}S \sim 0‰$) of sulfur in rainwater from Israel [*Herut et al.*, 1995], which implies efficient atmospheric mixing of the diverse anthropogenic sources.

[36] Analysis of the aerosol at Sde Boker using cascade impactors showed that most of the mineral dust in the fine fraction

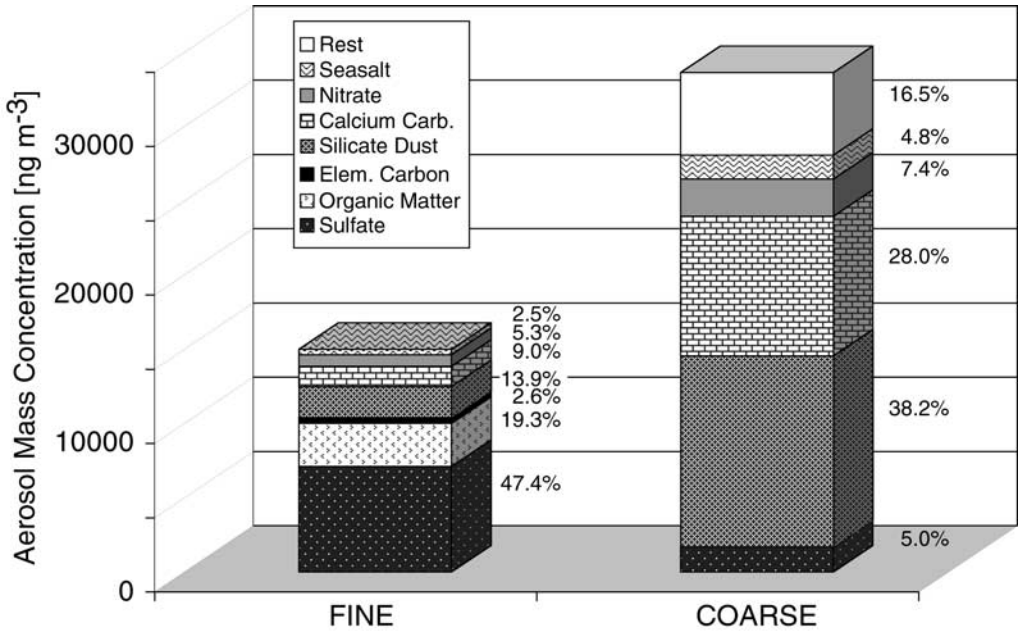

Figure 6. Average concentrations of the major constituents and chemical mass closure for the fine and coarse aerosols.

sample of the SFU (<2 μm) is present in the size range between 1 and 2 μm diameter [*Ichoku et al.*, 1999], and only a small amount of dust overlaps with the accumulation mode. Therefore in spite of the fact that our sampling site lies in a remote desert environment, it appears that for the fine mode we can draw similar conclusions as *Hegg et al.* [1997], who found that sulfates and carbonaceous aerosol species accounted for 90% of the dry aerosol mass for samples taken off the mid-Atlantic coast of the United States.

[37] On the other hand, the coarse mode at Sde Boker is dominated by silicate and calcium carbonate dust and contains minor amounts of nitrate, sulfate, and sea salt. Uptake of SO_2 and NO_xor HNO_3, and subsequent conversion to SO_4^{2-} and NO_3^- on the particle surfaces, occurs due to the alkalinity of soil dust, which can explain the presence of sulfate and nitrate associated with the dust particles [*Ganor and Pueschel*, 1988; *Dentener et al.*, 1996; *Levin et al.*, 1996; *Andreae and Crutzen*, 1997]. The presence of calcium sulfate and nitrate particles, presumably from the atmospheric conversion of $CaCO_3$ particles, was confirmed by single-particle analysis of aerosols collected at coastal and inshore locations in Israel [*Levin et al.*, 1996; *Ganor et al.*, 1998].

[38] For a mass apportionment of the various aerosol components, silicate dust was calculated by taking the geometric mean of Al (in ng m^{-3}) for the sampling period and dividing by the Al fraction in the average crustal rock (8.13%) [*Mason and Moore*, 1982]. In view of the large abundance of $CaCO_3$dust in the regional aerosol [*Ganor and Mamane*, 1982], sulfate and nitrate in the coarse fraction were assumed to be present as calcium sulfate and nitrate. $CaCO_3$ was estimated by first accounting for the Ca present in the silicate dust, using the composition of Mason's crustal average. Then the amount of Ca present as nitrate and sulfate was subtracted, and the remaining Ca was assumed to be in the form of $CaCO_3$. Sea salt was determined by first subtracting from total Na the amount of Na associated with the mineral dust (Na/Al = 0.348) and then dividing the remainder by the ratio of total salt to Na in seawater. Elemental carbon and organic matter were not considered for the coarse fraction, since no data were available to estimate their concentration. The unaccounted for remainder of the amount was determined by subtracting the sum of the above seven components from the total coarse particulate mass obtained gravimetrically. The rest obtained in this way, 17% of the coarse mass, may not be significant in view of analytical uncertainties and the variability in the possible composition of the mineral dust component. For example, if Fe or Ti is used instead of Al as the reference crustal element, no unaccounted for rest remains. Similarly, if the *Wedepohl* [1971] crustal composition is used, the calculated rest amount is insignificant. We conclude that given the uncertainties in the measurements and dust composition, we have satisfactory mass closure for the coarse aerosol.

3.4. Mass Scattering Efficiencies

[39] Aerosol composition at our site and the resulting light scattering is dominated by two aerosol types: soil dust in the coarse fraction, and anthropogenic sulfate and carbonaceous aerosol in the fine fraction. To quantify the optical effect of these aerosol components, we relate the observed scattering to the measured mass of CPM, FPM, dust, and sulfate. The fine and coarse particulate mass measurements for the period of 14 December 1995 until 9 October 1997 are shown in Figure 1c as time series plots. The FPM fraction is relatively constant; no obvious seasonal pattern is apparent from this time series plot. A more detailed analysis, however, shows that sulfate values are highest in summer, in agreement with the measurements made by *Luria et al.* [1996]. The CPM fraction shows prominent peaks from dust incidents. The low-dust months of July and August are evident for both years. The seasonal and interannual trends of chemical composition will be discussed in a future publication.

[40] Examination of the relationship between coarse aerosol and backscattering (Figure 7) shows a high correlation at high-dust loadings, when the effect of the dust aerosol is predominant. At CPM values less than ~100 μg m^{-3}, there is little relation between CPM and σ_{sp}, as the pollution aerosol dominates scattering in this regime. This is clearly seen in Figures 8 and 9, where total and backscattering are plotted against FPM. Both the total and the backscattering coefficients are strongly correlated with fine particulate mass, with the outliers being due to dust events with coarse mode fraction >60 μg m^{-3}.

[41] To analyze the relationships between scattering and the various measures of aerosol loading, we use the multivariate regression of σ_{sp} on CPM, FPM, sulfate, and dust concentrations to obtain spectral mass scattering efficiencies, α_X. This parameter, given in units of m^2 g^{-1}, is defined as the ratio of the light-

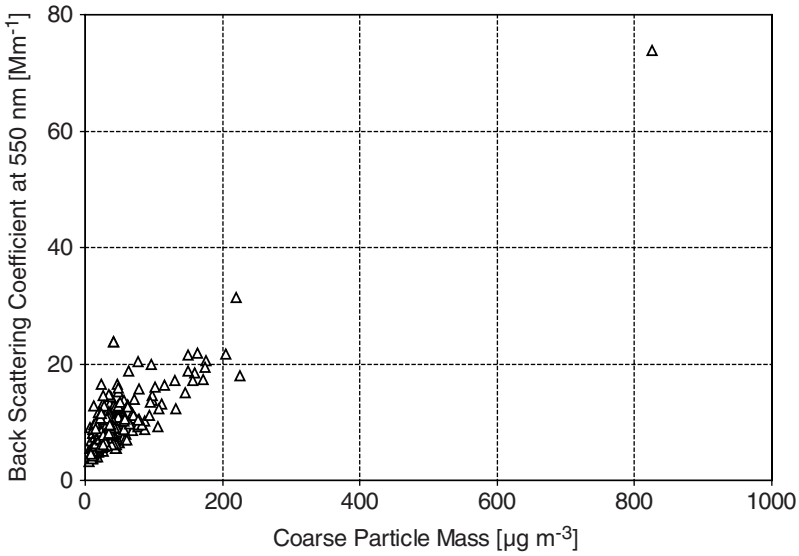

Figure 7. Scatterplot of the backscattering coefficient against the coarse particulate mass.

scattering coefficient, expressed in Mm^{-1}, to the aerosol mass concentration expressed in g m^{-3}. The use of this statistical approach to determine mass-scattering efficiencies, its prerequisites, and limitations have been discussed in the literature [e.g., *White*, 1986; *Vasconcelos et al.*, 2001]. To derive the α_λ for coarse and fine particle aerosols, as sampled by our SFU samplers, we have used the following model:

$$\sigma_{sp,\lambda} = k + \alpha_{\lambda,\mathrm{CPM}} * [\mathrm{CPM}] + \alpha_{\lambda,\mathrm{FPM}} * [\mathrm{FPM}],$$

where $\sigma_{sp,\lambda}$ is the aerosol scattering (Mm^{-1}) at wavelength λ, k is a constant representing contributions to scattering not related to either coarse or fine aerosol modes, $\alpha_{\lambda,\mathrm{CPM}}$ is the mass-scattering coefficient for coarse particulate mass at wavelength λ, and [CPM] and [FPM] are coarse and fine particulate mass concentrations (ng m^{-3}), respectively. For the regressions the nephelometer data were averaged over the same time periods over which the filter samples had been collected. The results of these calculations for total and backscattering and the three wavelengths measured by our instrument are presented in Table 4. The regressions are all significant at $p < 0.0001$, with r^2 around 0.8 in most cases. This implies that our model represents around 80% of variance, the rest probably due to a combination of variability in modal sizes and measurement uncertainties. The lowest r^2 values are found for dust, which has a high intrinsic variability in its optical properties, and for sulfate+, which represents a combination of sulfate with unspecified additional components (see below). The intercept $k$was computed in the regressions but is not considered further because it tended to be small and has no radiative significance. For total scattering we show the results based on both the uncorrected scattering coefficients as, provided by the TSI software, and the corrected σ_{sp} (in italics) obtained with the equations proposed by *Anderson and Ogren* [1998].

[42] While regression on CPM and FPM provides a convenient means of estimating the scattering efficiency due to the coarse and fine mode aerosol, it does not allow the rigorous separation of the scattering due to the actual aerosol size modes or the aerosol chemical components. This is because of the overlap of the dust

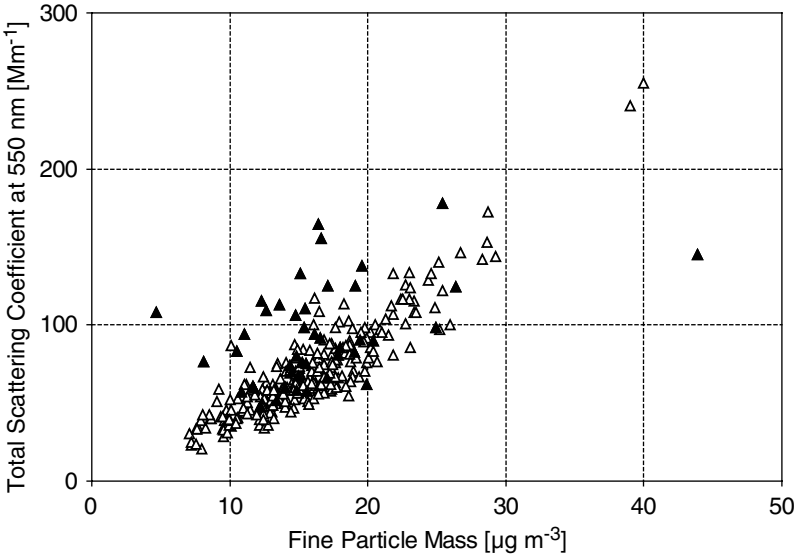

Figure 8. Scatterplot of the total scattering coefficient against the fine particulate mass. Solid triangles denote data with coarse particle mass >60 µg m^{-3}.

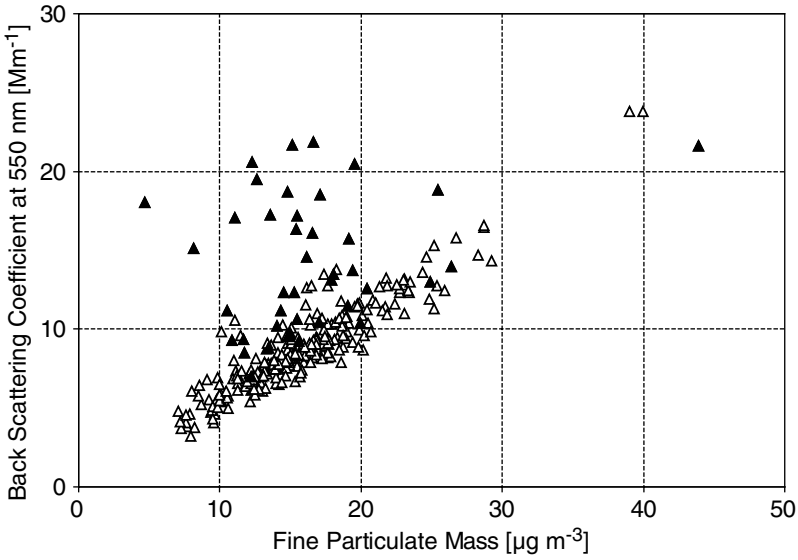

Figure 9. Scatterplot of the backscattering coefficient against the fine particulate mass. Solid triangles denote data with coarse particle mass >60 μg m^{-3}.

and sulfate size distributions across the size cut of the sampler [*White et al.*, 1994]. The size cut of the SFU at ~2 μm results in the presence of ~12–14% of the dust mode in the FPM sample (Table 3). Because of the increase of Mie-scattering efficiency at wavelengths close to those of the scattered radiation, the fine fraction of the dust aerosol has a relatively strong effect on scattering. Conversely, the relatively large fraction of anthropogenic sulfate and nitrate deposited on the dust aerosol adds only a minor contribution to total scattering. To separate the effects of the pollution and the mineral dust aerosol components, we have applied a number of different regression models (Table 4). As independent variables, we have used fine sulfate (fine-fraction S multiplied with 96.06/32.06), nonsulfate fine mass (FPM minus fine sulfate), and dust (silicate and carbonate, obtained from total (coarse plus fine) Al and Ca, using the same equations to derive silicate and carbonate dust as discussed above).

[43] Two types of $\alpha_{sulfate}$ are found in the literature: one is obtained by regression of σ_{sp} on sulfate alone, or on sulfate and a parameter representing coarse aerosol. In this case, $\alpha_{sulfate}$ contains the effect of all those constituents that correlate with sulfate, in particular the other anthropogenic components. Especially when large amounts of carbonaceous aerosol or ammonium nitrate are present, this results in high values of $\alpha_{sulfate}$, often higher than would be physically possible for pure sulfate particles [e.g., *ten Brink et al.*, 1996]. Alternatively, $\alpha_{sulfate}$ is calculated by accounting separately for all the aerosol components in the multivariate regression. This approach yields a scattering efficiency due to sulfate alone but requires that all components have been measured [*Charlson et al.*, 1999]. While we do not have measurements for all components in all samples of our time series, we have shown above that we are able to obtain excellent mass closure for our average composition using the combined information from the time series and intensive campaigns. We can therefore separate the effect of sulfate by using the following regression model, which contains both sulfate and nonsulfate fine mass:

$$\sigma_{sp,\lambda} = k + \alpha_{\lambda,\mathrm{CPM}}{}^{*}[\mathrm{CPM}] + \alpha_{\lambda,\mathrm{SO4}}{}^{*}[\mathrm{SO_4^{2-}}] + \alpha_{\lambda,\mathrm{FPM-SO4}}{}^{*}\left(\mathrm{FPM} - \left[\mathrm{SO_4^{2-}}\right]\right).$$

[44] For comparison with the literature, we have also computed this regression without the nonsulfate FPM term, which provides information on the scattering efficiency of the combination of sulfate itself and the other components statistically associated with it (termed $\alpha_{\lambda,\mathrm{sulfate+}}$ in Table 4). Finally, in an alternative analysis intended to characterize the α of the chemically defined dust component rather than the physically determined CPM, we have used

$$\sigma_{sp,\lambda} = k + \alpha_{\lambda,\mathrm{dust}}{}^{*}\,[\mathrm{Dust}] + \alpha_{\lambda,\mathrm{SO4}}{}^{*}\,[\mathrm{SO_4^{2-}}],$$

with the dust component computed as described above.

[45] A complication arises from the fact that our scattering measurements were made at a humidity lower than ambient (because of the elevated temperature in the nephelometer) but significantly greater than zero. The mean RH in the instrument was 38 ± 8% over the study period. To investigate the potential influence of humidity on aerosol size and scattering, we obtained Mie model calculations using the size-resolved composition obtained from 12-stage cascade impactor samples of the Sde Boker aerosol as input [*Maenhaut et al.*, 1996b] (A. Eldering, personal communication, 2000). These calculations suggest that water uptake at 50% RH, the humidity at which the samples were weighed, causes a mass increase of ~9%. For scattering, the model predicts an increase by ~6% at a humidity of 40%, a value close to the mean humidity in the nephelometer. Therefore the effects of humidity on mass and scattering almost cancel, leaving a possible underestimation of $\alpha_{\lambda,\mathrm{CPM}}$ and $\alpha_{\lambda,\mathrm{FPM}}$ by about 3%. On the other hand, since the measurements of the elemental concentrations are not influenced by humidity, while scattering may have increased by ~6% at the measurement RH of ~40%, the compound-specific $\alpha_{\lambda,\mathrm{SO4}}$ and $\alpha_{\lambda,\mathrm{Dust}}$ may have been overestimated by that percentage.

[46] The results in Table 4 show that the corrections for instrumental errors of the nephelometer have a significant effect on the magnitude of the α related to coarse particles, typically about 50%. For the fine aerosol components, the differences are minor, usually less than 10%, and typically about 5%. The truncation error dominates for the large particles and causes the large effect seen in our results for this size range. This error, however, applies only to the fraction of scattering very close to the direct beam and usually does not contribute significantly to the climatically relevant upscatter fraction (except when the Sun is very close to the horizon). We conclude therefore that the errors in radiative forcing estimates resulting from the instrument errors of the TSI 3563 are probably minor, of the order of 5%.

Table 4. Spectral Mass Scattering Coefficients Relating Scattering at Three Wavelengths (450, 550, and 700 nm) to Coarse Particulate Matter (CPM), Fine Particulate Matter (FPM), and Aerosol Sulfate on the Basis of Multivariate Regression Using 297 Samples[a]

	Spectral Mass-Scattering Coefficient (α_λ), m^2/g					
	$\alpha_{450\ nm}$	r^2	$\alpha_{550\ nm}$	r^2	$\alpha_{700\ nm}$	r^2
Total Scattering						
$\alpha_{\lambda,CPM}$	0.18 ± 0.03	0.76	0.31 ± 0.03	0.76	0.41 ± 0.02	0.78
	0.37 ± 0.04	*0.77*	*0.50 ± 0.03*	*0.77*	*0.57 ± 0.02*	*0.78*
$\alpha_{\lambda,Dust}$	0.46 ± 0.04	0.55	0.52 ± 0.03	0.54	0.53 ± 0.03	0.61
	0.67 ± 0.05	*0.54*	*0.71 ± 0.04*	*0.56*	*0.69 ± 0.04*	*0.64*
$\alpha_{\lambda,FPM}$	6.8 ± 0.2	0.76	5.2 ± 0.2	0.76	3.3 ± 0.1	0.78
	7.6 ± 0.3	*0.77*	*5.8 ± 0.2*	*0.77*	*3.7 ± 0.2*	*0.78*
$\alpha_{\lambda,SO4}$	8.1 ± 0.5	0.77	5.5 ± 0.4	0.76	2.8 ± 0.3	0.78
	8.4 ± 0.5	*0.77*	*5.6 ± 0.5*	*0.77*	*2.8 ± 0.4*	*0.78*
$\alpha_{\lambda,(FPM-SO4)}$	6.0 ± 0.4	0.77	5.0 ± 0.3	0.76	3.6 ± 0.2	0.78
	7.1 ± 0.4	*0.77*	*5.9 ± 0.3*	*0.77*	*4.2 ± 0.3*	*0.78*
$\alpha_{\lambda,sulfate+}$	11.0 ± 0.6	0.54	7.9 ± 0.5	0.52	4.6 ± 0.4	0.57
	11.8 ± 0.7	*0.53*	*8.4 ± 0.6*	*0.54*	*4.8 ± 0.5*	*0.60*
Backscattering						
$\alpha'_{\lambda,CPM}$	0.067 ± 0.003	0.84	0.074 ± 0.002	0.84	0.072 ± 0.001	0.84
$\alpha'_{\lambda,Dust}$	0.089 ± 0.004	0.69	0.090 ± 0.003	0.73	0.084 ± 0.003	0.76
$\alpha'_{\lambda,FPM}$	0.59 ± 0.02	0.84	0.46 ± 0.02	0.84	0.34 ± 0.02	0.84
$\alpha'_{\lambda,SO4}$	0.66 ± 0.04	0.84	0.51 ± 0.04	0.84	0.37 ± 0.03	0.84
$\alpha'_{\lambda,(FPM-SO4)}$	0.54 ± 0.03	0.84	0.43 ± 0.03	0.84	0.33 ± 0.02	0.84
$\alpha'_{\lambda,sulfate+}$	0.92 ± 0.05	0.67	0.71 ± 0.05	0.72	0.52 ± 0.04	0.75

[a] Values in italics are based on scattering data corrected for non-Lambertian behavior and truncation errors of the nephelometer.

[47] When comparing $\alpha_{\lambda,CPM}$ (scattering due to the aerosol mass >2 μm) and $\alpha_{\lambda,Dust}$ (scattering due to the chemically determined dust fraction), we see significant differences. First, $\alpha_{\lambda,Dust}$is considerably larger, some 40% at 550 nm, suggesting that dust in the size fraction <2 μm makes a significant contribution to the scattering by mineral dust overall. Second, we find that there is little spectral dispersion in $\alpha_{\lambda,Dust}$, while $\alpha_{\lambda,CPM}$ has a distinct, negative "Ångström coefficient," reflecting the fact that $\alpha_{\lambda,CPM}$ only includes the larger part of the dust mode. Similarly, the Ångström coefficient of $\alpha_{\lambda,SO4}$ (2.40) is considerably larger than that of $\alpha_{\lambda,FPM}$ (1.64), since the latter represents a mixture of the effects of fine-mode sulfate and the lower tail of the dust mode. These comparisons show that caution should be used when interpreting radiative properties on the basis of size segregation alone as representative of specific aerosol components. They also highlight the fact that the <2μm fraction of the dust mode should not be ignored in the analysis of the dust climatic effect, as sometimes is done in climate models.

[48] In Table 5 we compare our mass scattering efficiency results to values found in the literature. For these comparisons, we use the uncorrected values, since they most closely correspond to those reported previously. It is important to note that because of differences in the sampling and analysis regimes, such as the size cutoff for the fine and coarse mode, the humidity of the sampled air, and the chemical apportionment of the aerosols, the calculated α values are not always directly comparable. Our sulfate-scattering efficiency, $\alpha_{550,SO4}$ = 5.5, falls within the range reported for low-humidity conditions by other authors and coincides with the theoretically predicted value for sulfate particles with a diameter of 0.4–0.5 μm [*Charlson et al.*, 1999]. In contrast, our mass-scattering efficiency of 5.2 $m^2\ g^{-1}$ for total FPM, $\alpha_{550,FPM}$, is above the range of literature values (2.4 to 4.7 $m^2\ g^{-1}$). This discrepancy may be partially due to differences in cutoff size, since the frequently used cutoff at 2.5 μm would result in more dust aerosol being included and therefore a lower α. Another factor is the size of the fine aerosol at Sde Boker, which because of its aged character is relatively large. The sulfate mass median diameter is around 0.4–0.5 μm and therefore near the maximum in the scattering efficiency/size relationship [*Charlson et al.*, 1999]. In studies conducted in or near urban regions, such as those by *Dzubay et al.* [1982], *White et al.* [1994], or *Hegg et al.* [1995], the effective fine aerosol diameter is often only about half that typical of our region. Finally, since sulfate dominates the composition of the fine aerosol at Sde Boker, it is to be expected that sulfate and fine-mass α have similar values.

[49] When nonsulfate but correlated compounds were not accounted for separately in the regressions, the reported values for $\alpha_{550,sulfate+}$, range from 2 to 26.3 $m^2\ g^{-1}$. Our value of $\alpha_{550,sulfate+}$ = 7.9 $m^2\ g^{-1}$ is consistent with the fact that sulfate dominates the anthropogenic aerosol with about 64% and that other components make only modest contributions to scattering. Literature values much higher than ours often include the effects of humidity or large amounts of ammonium nitrate. *Clarke et al.* [1996b] for their range of 5–16 $m^2\ g^{-1}$ for SO_4^{2-} discuss the effect of humidity on α. Their highest value of 16 $m^2\ g^{-1}$ is for surface samples taken in very moist air. The value of 5 $m^2\ g^{-1}$ is for samples taken at several kilometers in altitude, where humidity is lower. For surface samples taken in the Netherlands on the North Sea coast, *ten Brink et al.* [1996] report 20 $m^2\ g^{-1}$ for $\alpha_{550,sulfate+}$, indicative in this case of a larger contribution of nitrate than sulfate to the aerosol light scattering.

[50] The literature values for the coarse mode α fall in the range of 0.34–1.1 $m^2\ g^{-1}$. Our values of $\alpha_{550,CPM}$ = 0.31 $m^2\ g^{-1}$and $\alpha_{550,Dust}$ = 0.52 $m^2\ g^{-1}$ are in the lower part of this range and close to the range of 0.34–0.45 $m^2\ g^{-1}$ reported for the southwestern United States [*White et al.*, 1994]. The values of 1.1 and 0.83 $m^2\ g^{-1}$ reported for aged dust over the Atlantic Ocean [*Clarke et al.*, 1996a] and at Barbados [*Li et al.*, 1996] are higher than our value. This is most likely because the aged dust at these sites has shifted to smaller sizes, resulting in a higher scattering efficiency.

3.5. Contributions of Dust and Anthropogenic Aerosols to Surface-Level Scattering at Sde Boker

[51] The time series of calculated total scattering at 550 nm due to the anthropogenic and dust aerosols for this study is presented in Figure 1d. Scattering due to the anthropogenic fraction was calculated using sulfate as a proxy for the anthropogenic component and $\alpha_{550,sulfate+}$ = 7.9 $m^2\ g^{-1}$ to take the effect of additional sulfate-correlated components also into account. Dust scattering was estimated using the estimate of dust mass calculated from Al

Table 5. Estimates of Mass-Scattering Efficiencies for Four Categories of Aerosol. Sulfate+ Refers to Scattering From SO_4^{2-} and Other Correlated Aerosol Components Present in the Sampled Air

General Location	Year	Altitude	α_{550}, $m^2\ g^{-1}$				Reference
			Fine	Coarse	SO_4^{2-}	Sulfate+	
Southern Sweden	1973–1974	aircraft	...	...	...	5 ± 2 (450nm)	*Waggoner et al.* [1976]
New York City, New York, USA	1976–1977	surface	...	...	8.8 ± 0.5	...	*Leaderer et al.* [1981]
...	...	...	3.1 ± 0.2	...	...	...	*Waggoner et al.* [1981]
Houston, Texas, USA	...	surface	3.5	...	...	...	*Dzubay et al.* [1982]
Canadian Arctic	1979–1984	surface	...	...	10.9 ± 1.1	...	*Barrie and Hoff* [1985]
Maryland, Long Island, USA	1980–1983	aircraft	...	...	...	12.0 ± 1.4	*ten Brink et al.* [1987]
Eastern USA	...	surface	...	...	5	...	*White et al.* [1990]
...	...	...	...	...	5	8.5	*Charlson et al.* [1991, 1992]
NE Atlantic, Azores Islands	1992	0-2.7 km	...	...	2.8 ± 0.14	2-26.3	*Hegg et al.* [1993]
Southwest USA	1989	surface	2.4-2.5	0.34-0.45	...	...	*White et al.* [1994]
NE Atlantic seaboard	1993	0.3-2 km	3.2	...	2.2 ± 0.4	2.1 ± 0.8	*Hegg et al.* [1995]
Pacific Ocean	1991–1992	surface	...	...	3.6 ± 1.1	...	*Quinn et al.* [1995]
NE Atlantic (ASTEX)	...	0-3 km	4.0 ± 0.7	1.1 ± 0.2	~5	5-16	*Clarke et al.* [1996a]
Barbados	1994	surface	...	0.83 ± 0.4	...	...	*Li et al.* [1996]
Pacific Ocean	1993–1994	surface	...	...	4.3-7.5	...	*Quinn et al.* [1996]
North Sea, Netherlands	1993	surface	...	...	...	20	*ten Brink et al.* [1996]
Mid-Atlantic coast, USA	1996	0-4 km	2.8	...	2.7 ± 1.3	...	*Hegg et al.* [1997]
Hungary, rural winter	1994–1995	surface	...	...	8.3	...	*Meszaros et al.* [1998]
Hungary, rural summer	1995	surface	...	...	5.9 ± 2	...	*Meszaros et al.* [1998]
Negev desert, Israel, winter	1997	surface	3.7 ± 0.6	0.12 ± 0.05	...	...	*Ichoku et al.* [1999]
Negev desert, Israel, summer	1996	surface	...	...	7.4 ± 2.0	...	*Formenti et al.* [2001b]
Negev desert, Israelx	1995–1997	surface	5.2	0.31	5.5	7.9	Andreae et al., this work

and Ca and $\alpha_{550,Dust} = 0.52\ m^2\ g^{-1}$. The model predicts a median σ_{sp} over the time period of this study of 64.5 Mm^{-1}, almost identical to the observed median of 66.7 Mm^{-1}. Sulfate alone accounts for 50% (32.2 Mm^{-1}), and the total anthropogenic fraction for 72% (46.2 Mm^{-1}) of the scattering at Sde Boker. Figure 1d illustrates the dominant effect of the anthropogenic aerosol in the form of a time series. The scattering due to dust is lower throughout, reaching the levels produced by the anthropogenic component only during dust events. In the summer there is a noticeable maximum of pollution-derived scattering, while the scattering from dust in this season is low and free of major peaks, reflecting the low incidence of dust storms.

[52] For an alternative approach to estimating the anthropogenic contribution to scattering, we have calculated σ_{sp} at 550 nm due to CPM and FPM using $\alpha_{550,FPM}$ and $\alpha_{550,CPM}$ and the corresponding mass loadings. From this model, we obtain a contribution of 80% due to the fine fraction. If we use the sum of the mean mass values for SO_4^{2-}, NO_3^-, organic matter, and elemental carbon (Table 3) as a proxy for pollution-derived aerosols, we estimate that ~80% of the fine fraction mass is anthropogenic, and consequently, ~64% of scattering is due to anthropogenic aerosol. Since the anthropogenic fraction is highest in summer, when the solar zenith angle is low, the radiative effect of this anthropogenic perturbation is even greater than the effect on annual mean scattering.

4. Conclusions

[53] In a 2 year study of the chemical and physical properties of the aerosol at Sde Boker, a remote site in the Negev desert, Israel, we found that the region receives substantial amounts of pollution aerosols, in addition to mineral dust aerosols from the surrounding deserts. The concentrations of combustion-related pollutants, such as sulfate and black carbon aerosols, as well as the levels of light scattering by aerosols were in the range typical of industrialized and highly populated regions, such as western Europe or the Los Angeles air basin. Consistent with the findings made previously in this region, we can attribute most of the pollution aerosol to long-range transport from central and eastern Europe, as well as southern Russia [*Luria et al.*, 1996; *Maenhaut et al.*, 1997; *Ichoku et al.*, 1999; *Formenti et al.*, 2001a, 2001b]. While there are substantial regional emissions of SO_2, especially along the Israeli coast [*Peleg et al.*, 1994], there is usually not enough time for them to become transformed to sulfate aerosol by the time the air masses reach our site in the Negev desert [*Ichoku et al.*, 1999; *Formenti et al.*, 2001b].

[54] Mineral dust dominates the aerosol mass burden at the site, accounting for about 74% of TPM on average. Much of this dust loading occurs during seasonal and diurnal dust events, as shown by the fact that the median CPM concentration (32 $\mu g\ m^{-3}$) is considerably smaller than the average value (44 $\mu g\ m^{-3}$). However, in spite of the desert location and the large contribution of mineral dust to the aerosol mass burden, the fine-mode aerosol plays a dominant role in the optical characteristics of the atmosphere in the study region. We find that aerosol light scattering intensity is very strongly correlated with fine aerosol mass concentration, except during dust events. The Ångström coefficient (median 1.52) also shows the dominant influence of fine-mode particles. While the results presented in this paper strictly refer to conditions at ground level, *Formenti et al.* [2001a, 2001b] have shown with Sun photometer data that the optical properties and size distributions of the aerosol are similar aloft.

[55] The fine mode aerosol consists predominately of sulfate and carbonaceous particles, which are almost exclusively anthropogenic. Nitrate, dust, and sea salt are present as minor components in the fine fraction. Approximately 80% of the fine mode can be attributed to anthropogenic emissions, while the rest mostly consists of the fine tail of the dust size distribution. The aerosol in the coarse mode consists of silicate and carbonate dust, with some additional nitrate, sulfate, and sea salt. Coarse nitrate and sulfate are probably present as a result of the deposition or reaction of acidic species (SO_2, H_2SO_4, NO_x, HNO_3) on the alkaline dust particles. Excellent mass closure was obtained for the fine fraction, while the measured aerosol species could only account for 83% of the CPM determined by weighing. This difference may, however, not be significant in view of the uncertainties involved.

[56] Mass-scattering efficiencies for the fine and coarse fractions and the sulfate-scattering efficiency were obtained by multivariate regression. The values at Sde Boker are at the high end of the range of previous observations, probably because the aerosol is in the size range most effective for light scattering. The sulfate

mass median diameter is around 0.4–0.5 μm, consistent with the highly aged nature of the aerosol. Since much of the direct effect of anthropogenic aerosols is caused by similarly aged aerosols, our α values may be more applicable to radiative forcing calculations than the lower values obtained closer to sources.

[57] From the mass scattering efficiencies and the time series of the aerosol mass fractions, we can calculate the annual mean contributions of the anthropogenic and dust fractions to light scattering at Sde Boker. We find that on the long-term average, about 70% of the scattering coefficient can be attributed to the anthropogenic component. The annually integrated effect of the anthropogenic component on aerosol radiative forcing is even stronger than this number suggests, because of the parallel seasonality of the radiative flux and the relative and absolute abundance of anthropogenic aerosol. Much of the contribution of the coarse mode aerosol occurs during relatively few dust events, mostly in winter and spring. In contrast, the anthropogenic scattering component is highest in summer (58.6 Mm^{-1}, or 77% of total σ_{sp}), when radiative fluxes are also highest.

[58] The observed sulfate concentrations (mean, 7.1 μg m^{-3}) are consistent with model predictions for the study region [*Langner and Rodhe*, 1991; *Pham et al.*, 1995; *Chin and Jacob*, 1996]. Our observations show that long-range transport of pollutants from Europe and Russia has a large-scale impact on aerosol concentrations and aerosol radiative forcing. Additional source regions may be in Africa and Asia, but their impact on the Near East region remains to be quantified (G.-J. Roelofs, personal communication, 1999).

[59] To obtain an initial, rough estimate of the radiative forcing by anthropogenic aerosols in the study region, we estimate the radiative forcing efficiency (RFE) at the top of the atmosphere (TOA), i.e., the amount of radiative forcing corresponding to a unity increase in aerosol optical thickness using the equation given by *Anderson et al.* [1999], based on the analysis of *Haywood and Shine* [1995]:

$$\mathrm{RFE} = S \cdot D(1 - A_c)T^2(1 - R_s)^2 \left[2R_s \frac{1 - \omega}{(1 - R_s)^2} - \beta(b)\omega \right]$$

where RFE and the solar constant S have units of W m^{-2} (S = 1370 W m^{-2}), D is the daylight fraction (set to 0.5), and T is the atmospheric transmissivity (0.76). The mean fractional cloud cover, A_c, for our region is 0.29 [*Warren et al.*, 1986], and the surface albedo ranges (R_s) from 0.07 (ocean) to 0.35 (desert). The average upscatter fraction $\beta(b)$ was derived from the backscatter ratio, b, using the polynomial $\beta = 0.082 + 1.85b - 2.97b^2$, which closely approximates the relationship for a Heyney-Greenstein phase function [*Anderson et al.*, 1999]. Measurements made during the ARACHNE-96 campaign suggested a mean value of 0.92 ± 0.03 for the single-scattering albedo (ω) of the aerosol at Sde Boker [*Formenti et al.*, 2001b]. The use of the value from this campaign as an estimate for the overall average is a reasonable assumption, since the BCE/FPM ratio during this campaign (0.080 ± 0.017) was very close to the long-term average (0.081 ± 0.029). Since we are most interested in the radiative effects of the anthropogenic component, we ignore the long-wave forcing due to dust and the effect of high optical thickness during dust storms.

[60] From these data, we obtain a RFE of −12.8 W m^{-2} over land and −55.2 W m^{-2} over the sea. Using the long-term average aerosol optical thickness (AOT) at 670 nm measured at Sde Boker of 0.16 [*Holben et al.*, 2001] and a 70% anthropogenic contribution to AOT based on the above discussion, we obtain TOA forcing estimates of −1.4 and −6.2 W m^{-2} over land and sea, respectively. (We have neglected here the slight spectral dependence of the aerosol optical properties, b and ω, and have chosen AOT at 670 nm to approximate the mean solar spectrum).

[61] As an alternative to this rough estimate of radiative forcing, we computed the TOA forcing due to the anthropogenic aerosol using the streamer radiative code [*Key and Schweiger*, 1998] for the same aerosol optical depth and the aerosol optical properties derived from our measurements. The wavelength dependence of the aerosol optical depth was inferred from the wavelength dependence of the mass-scattering efficiency of the fine mode (Table 4) and extrapolated below 450 and above 700 nm assuming a constant Ångström coefficient across the wavelength intervals 250–550 nm and 550–4000 nm. The single-scattering albedo of 0.92 at 550 nm was extrapolated to other wavelengths following the wavelength dependence measured by *Dubovik et al.* [2001] for pollution aerosols. The asymmetry parameter was prescribed to typical values computed for fine-mode particles from Mie theory, in broad agreement with the measured backscatter fractions (Table 2). The wavelength-dependent surface reflectance for ocean and desert (dry sand) was assumed to be Lambertian, and we prescribed a uniform aerosol layer in the boundary layer. The annually averaged clear-sky radiative forcing amounts to −3.5 and −6.2 W m^{-2} over desert and ocean surfaces, respectively. Assuming a negligible aerosol direct effect in cloudy sky and using the climatological mean cloud cover of 29%, this translates into an all-sky radiative forcing of −2.5 and −4.9 W m^{-2} over desert and ocean surfaces, respectively.

[62] Both the crude estimate, based on the formula of *Anderson et al.* [1999], and the detailed radiative transfer calculation are in good agreement with predictions from global models of aerosol radiative forcing. For example, *Haywood and Shine* [1995] predicted a TOA forcing of −2 to −3 W m^{-2} for our study region (without explicitly distinguishing between land and sea areas), using the sulfate distribution from the *Langner and Rodhe* [1991] model and a soot/sulfate mass ratio of 0.075.

[63] For further comparison with model predictions of forcing, we can estimate the sulfate forcing alone. Assuming that scattering accounts for 92% of AOT (ω = 0.92), that sulfate contributes the same fraction to AOT as to σ_{sp} (50%), and taking the single-scattering albedo of sulfate as 1.0, we obtain a sulfate forcing of −2.3 and −4.7 W m^{-2} over land and sea, respectively. These values are in good agreement with the model predictions for climate forcing due to sulfate in our region, which fall in the range of −2 to −5 W m^{-2} [*Charlson et al.*, 1991; *Boucher and Anderson*, 1995; *Feichter et al.*, 1997; *Langmann et al.*, 1998; *Penner et al.*, 1998]. Overall, we conclude that our data provide strong support for a negative radiative forcing due to anthropogenic aerosols in the eastern Mediterranean region, and that the magnitude of this forcing is in good agreement with current model predictions.

[64] **Acknowledgments.** We thank A. Eldering for making model calculations to estimate the effects of humidity changes on aerosol composition and light scattering. P. Formenti, H. Gimm, F. Meixner, and B. Stunder are acknowledged for help in producing the back trajectories. An anonymous reviewer made the valuable suggestion to include the results of a radiative transfer calculation. We thank R. J. Charlson for valuable comments on the manuscript and O. Boucher for performing the radiative transfer calculations. This research was supported by the Max Planck Society, Germany, and by the Belgian Federal Office for Scientific, Technical and Cultural Affairs, the Special Research Fund of the University of Gent, and the Fonds voor Wetenschappelijk Onderzoek-Vlaanderen.

References

Anderson, T. L., and J. A. Ogren, Determining aerosol radiative properties using the TSI 3563 integrating nephelometer, *Aerosol Sci. Technol.*, *29*, 57–69, 1998.

Anderson, T. L., et al., Performance characteristics of a high-sensitivity, three- wavelength, total scatter/backscatter nephelometer, *J. Atmos. Oceanic. Technol.*, *13*, 967–986, 1996.

Anderson, T. L., D. S. Covert, J. D. Wheeler, J. M. Harris, K. D. Perry, B. E. Trost, D. J. Jaffe, and J. A. Ogren, Aerosol backscatter fraction and single-scattering albedo: Measured values and uncertainties at a coastal station in the Pacific Northwest, *J. Geophys. Res.*, *104*, 26,793–26,807, 1999.

Andreae, M. O., Soot carbon and excess fine potassium: Long-range transport of combustion-derived aerosols, *Science*, *220*, 1148–1151, 1983.

Andreae, M. O., Climatic effects of changing atmospheric aerosol levels, in *World Survey of Climatology*, vol. 16, *Future Climates of the World*, edited by A. Henderson-Sellers, pp. 341–392, Elsevier Sci., New York, 1995.

Andreae, M. O., and P. J. Crutzen, Atmospheric aerosols: Biogeochemical sources and role in atmospheric chemistry, *Science*, *276*, 1052–1056, 1997.

Andreae, M. O., T. W. Andreae, R. J. Ferek, and H. Raemdonck, Long-range transport of soot carbon in the marine atmosphere, *Sci. Total Environ.*, *36*, 73–80, 1984.

Barrie, L. A., and R. M. Hoff, Five years of air chemistry observations in the Canadian Arctic, *Atmos. Environ.*, *19*, 1995–2010, 1985.

Beck, W., and H. Engelhardt, Capillary electrophoresis of organic and inorganic cations with indirect UV detection, *Chromatographia*, *33*, 313–316, 1992.

Bodhaine, B. A., N. C. Ahlquist, and R. C. Schnell, Three-wavelength nephelometer suitable for aircraft measurement of background aerosol scattering coefficient, *Atmos. Environ. Ser. A*, *25*, 2267–2276, 1991.

Boucher, O., and T. L. Anderson, General circulation model assessment of the sensitivity of direct climate forcing by anthropogenic sulfate aerosols to aerosol size and chemistry, *J. Geophys. Res.*, *100*, 26,117–26,134, 1995.

Cahill, T. A., R. A. Eldred, P. J. Feeney, P. J. Beveridge, and L. K. Wilkinson (Eds.), in *The Stacked Filter Unit Revisited*, Air and Waste Manage. Assoc., Pittsburgh, Pa., 1990.

Caldow, R., F. R. Quant, R. L. Holm, and G. J. Sem, A three-wavelength high-sensitivity integrating nephelometer with backscatter operation, paper presented at the 1994 Fourth International Aerosol Conference, Los Angeles, Ca., 1994.

Chanin, M.-L., New issues on climate change forcings, *Eur. Rev.*, *4*, 143–164, 1996.

Charlson, R. J., J. Langner, H. Rodhe, C. B. Leovy, and S. G. Warren, Perturbation of the northern hemisphere radiative balance by backscattering from anthropogenic sulfate aerosols, *Tellus, Ser. AB*, *43*, 152–163, 1991.

Charlson, R. J., S. E. Schwartz, J. M. Hales, R. D. Cess, J. A. Coakley, J. E. Hansen, and D. J. Hofmann, Climate forcing by anthropogenic aerosols, *Science*, *255*, 423–430, 1992.

Charlson, R. J., T. L. Anderson, and H. Rodhe, Direct climate forcing by anthropogenic aerosols: Quantifying the link between atmospheric sulfate and radiation, *Contrib. Atmos. Phys.*, *72*, 79–94, 1999.

Chin, M., and D. Jacob, Anthropogenic and natural contributions to atmospheric sulfate: A global model analysis, *J. Geophys. Res.*, *101*, 18,691–18,699, 1996.

Claquin, T., M. Schulz, Y. Balkanski, and O. Boucher, Uncertainties in assessing radiative forcing by mineral dust, *Tellus, Ser. B*, *50*, 491–505, 1998.

Clarke, A. D., J. N. Porter, F. P. J. Valero, and P. Pilewskie, Vertical profiles, aerosol microphysics, and optical closure during the Atlantic Stratocumulus Transition Experiment: Measured and modeled column optical properties, *J. Geophys. Res.*, *101*, 4443–4453, 1996a.

Clarke, A. D., T. Uehara, and J. N. Porter, Lagrangian evolution of an aerosol column during the Atlantic Stratocumulus Transition Experiment, *J. Geophys. Res.*, *101*, 4351–4362, 1996b.

Cornille, P., W. Maenhaut, and J. M. Pacyna, Sources and characteristics of the atmospheric aerosol near Damascus, Syria, *Atmos. Environ., Ser. A*, *24*, 1083–1093, 1990.

Dayan, U., Climatology of back trajectories from Israel based on synoptic analysis, *J. Appl. Meteorol.*, *25*, 591–595, 1986.

Dentener, F. J., G. R. Carmichael, Y. Zhang, J. Lelieveld, and P. J. Crutzen, Role of mineral aerosol as a reactive surface in the global troposphere, *J. Geophys. Res.*, *101*, 22,869–22,889, 1996.

Dubovik, O., B. N. Holben, T. F. Eck, A. Smirnov, Y. J. Kaufman, M. D. King, D. Tanré, and I. Slutsker, Variability of absorption and optical properties of key aerosol types observed in worldwide locations, *J. Geophys. Res.*, in press, 2001.

Dzubay, T. G., R. K. Stevens, C. W. Lewis, D. H. Hern, W. J. Courtney, J. W. Tesch, and M. A. Mason, Visibility and aerosol composition in Houston, Texas, *Environ. Sci. Technol.*, *16*, 514–525, 1982.

Feichter, J., E. Kjellström, H. Rodhe, F. Dentener, J. Lelieveld, and G.-J. Roelofs, Simulation of the tropospheric sulfur cycle in a global climate model, *Atmos. Environ.*, *30*, 1693–1707, 1996.

Feichter, J., U. Lohmann, and I. Schult, The atmospheric sulfur cycle in ECHAM-4 and its impact on the shortwave radiation, *Clim. Dyn.*, *13*, 235–246, 1997.

Formenti, P., et al., Aerosol optical properties and large-scale transport of air masses: Observations at a coastal and a semiarid site in the eastern Mediterranean during summer 1998, *J. Geophys. Res.*, *106*, 9807–9826, 2001a.

Formenti, P., et al., Physical and chemical characteristics of aerosols over the Negev desert (Israel) during summer 1996, *J. Geophys. Res.*, *106*, 4871–4890, 2001b.

Fuller, K. A., W. C. Malm, and S. M. Kreidenweis, Effects of mixing on extinction by carbonaceous particles, *J. Geophys. Res.*, *104*, 15,941–15,954, 1999.

Ganor, E., The frequency of Saharan dust episodes over Tel Aviv, Israel, *Atmos. Environ.*, *28*, 2867–2871, 1994.

Ganor, E., and Y. Mamane, Transport of Saharan dust across the eastern Mediterranean, *Atmos. Environ.*, *16*, 581–587, 1982.

Ganor, E., and R. F. Pueschel, Composition of individual nitrate containing particles in non-urban atmospheres of Colorado, USA and Tel Aviv, Israel, *Water Air Soil Pollut.*, *42*, 169–181, 1988.

Ganor, E., H. A. Foner, S. Brenner, E. Neeman, and N. Lavi, The chemical composition of aerosols settling in Israel following dust storms, *Atmos. Environ., Ser. A*, *25*, 2665–2670, 1991.

Ganor, E., Z. Levin, and R. Van Grieken, Composition of individual aerosol particles above the Israelian Mediterranean Coast during the summer time, *Atmos. Environ.*, *32*, 1631–1642, 1998.

Ginoux, P., M. Chin, I. Tegen, J. Herman, O. Torres, and B. Holben, Global modeling of mineral dust with the Goddard transport model, paper presented at the Workshop on Mineral Dust, Boulder, Colo., 1999.

Gray, H. A., G. R. Cass, J. J. Huntzicker, E. K. Heyerdahl, and J. A. Rau, Characteristics of atmospheric organic and elemental carbon particle concentrations in Los Angeles, *Environ. Sci. Technol.*, *20*, 580–589, 1986.

Groblicki, P. J., G. T. Wolff, and R. J. Countess, Visibility-reducing species in the Denver "brown cloud," I, Relationships between extinction and chemical composition, *Atmos. Environ.*, *15*, 2473–2484, 1981.

Guelle, W., Y. J. Balkanski, M. Schulz, B. Marticorena, G. Bergametti, C. Moulin, R. Arimoto, and K. D. Perry, Modeling the atmospheric distribution of mineral aerosol: Comparison with ground measurements and satellite observations for yearly and synoptic timescales over the North Atlantic, *J. Geophys. Res.*, *105*, 1997–2012, 2000.

Güllü, G. H., I. Ölmez, S. Aygün, and G. Tuncel, Atmospheric trace element concentrations over the eastern Mediterranean Sea: Factors affecting temporal variability, *J. Geophys. Res.*, *103*, 21,943–21,954, 1998.

Haywood, J. M., and K. P. Shine, The effect of anthropogenic sulfate and soot aerosol on the clear-sky planetary radiation budget, *Geophys. Res. Lett.*, *22*, 603–606, 1995.

Hegg, D. A., R. J. Ferek, and P. V. Hobbs, Light scattering and cloud condensation nucleus activity of sulfate aerosol measured over the Northeast Atlantic Ocean, *J. Geophys. Res.*, *98*, 14,887–14,894, 1993.

Hegg, D. A., P. V. Hobbs, R. J. Ferek, and A. P. Waggoner, Measurements of some aerosol properties relevant to radiative forcing on the east coast of the United States, *J. Appl. Meteorol.*, *34*, 2306–2315, 1995.

Hegg, D. A., P. V. Hobbs, S. Gasso, J. D. Nance, and A. L. Rangno, Aerosol measurements in the Arctic relevant to direct and indirect radiative forcing, *J. Geophys. Res.*, *101*, 23,349–23,363, 1996.

Hegg, D. A., J. Livingston, P. V. Hobbs, T. Novakov, and P. Russell, Chemical apportionment of aerosol column optical depth off the mid-Atlantic coast of the United States, *J. Geophys. Res.*, *102*, 25,293–25,303, 1997.

Heidam, N. Z., Review: Aerosol fractionation by sequential filtration with Nuclepore filters., *Atmos. Environ.*, *15*, 891, 1981.

Herut, B., B. Spiro, A. Starinsky, and A. Katz, Sources of sulfur in rainwater as indicated by isotopic delta^{34}S data and chemical composition, Israel, *Atmos. Environ.*, *29*, 851–857, 1995.

Holben, B. N., et al., An emerging ground-based aerosol climatology: Aerosol optical depth from AERONET, *J. Geophys. Res.*, *106*, 12,067–12,097, 2001.

Houghton, J., Y. Ding, D. J. Griggs, M. Noguer, P. J. van der Linden, X. Dai, K. Maskell, and C. A. Johnson (Eds.), *Climate Change: The Scientific Basis*, Cambridge Univ. Press, New York, 2001.

Houghton, J. T., L. G. Meira Filho, B. A. Callander, N. Harris, A. Kattenberg, and K. Maskell (Ed.), *Climate Change, 1995: The Science of Climate Change*, 572 pp., Cambridge Univ. Press, New York, 1996.

Ichoku, C., et al., Interrelationships between aerosol characteristics and light scattering in an eastern Mediterranean arid environment, *J. Geophys. Res.*, *104*, 24,371–24,393, 1999.

John, W., S. Hering, G. Reischl, G. Sasaki, and S. Goren, Characteristics of Nuclepore filters with large pore size, II, Filtration properties, *Atmos. Environ.*, *17*, 373–382, 1983.

Key, J., and A. J. Schweiger, Tools for atmospheric radiative transfer: Streamer and Fluxnet, *Comput. Geosci.*, *24*, 443–451, 1998.

Kiehl, J. T., and B. P. Briegleb, The relative role of sulfate aerosols and greenhouse gases in climate forcing, *Science*, *260*, 311–314, 1993.

Kubilay, N., and A. C. Saydam, Trace elements in atmospheric particulates over the eastern Mediterranean; concentrations, sources, and temporal variability, *Atmos. Environ.*, *29*, 2289–2300, 1995.

Langmann, B., M. Herzog, and H. F. Graf, Radiative forcing of climate by sulfate aerosols as determined by a regional circulation chemistry transport model, *Atmos. Environ.*, *32*, 2757–2768, 1998.

Langner, J., and H. Rodhe, A global three-dimensional model of the tropospheric sulfur cycle, *J. Atmos. Chem.*, *13*, 255–263, 1991.

Langner, J., H. Rodhe, P. J. Crutzen, and P. Zimmermann, Anthropogenic influence on the distribution of tropospheric sulphate aerosol, *Nature*, *359*, 712–716, 1992.

Leaderer, B. P., R. L. Tanner, P. J. Lioy, and J. A. J. Stolwijk, Seasonal variations in light scattering in the New York region and their relation to sources, *Atmos. Environ.*, *15*, 2407–2420, 1981.

Levin, Z., and J. D. Lindberg, Size distributions, chemical composition, and optical properties of urban and desert aerosols in Israel, *J. Geophys. Res.*, *84*, 6941–6950, 1979.

Levin, Z., E. Ganor, and V. Gladstein, The effect of desert particles coated with sulfate on rain formation in the eastern Mediterranean, *J. Appl. Meteorol.*, *35*, 1511–1523, 1996.

Li, X., H. Maring, D. Savoie, K. Voss, and J. M. Prospero, Dominance of mineral dust in aerosol light-scattering in the North Atlantic trade winds, *Nature*, *380*, 416–419, 1996.

Luria, M., M. Peleg, G. Sharf, D. S. Tov-Alper, N. Spitz, Y. Ben Ami, Z. Gawii, B. Lifschitz, A. Yitzchaki, and I. Seter, Atmospheric sulfur over the east Mediterranean region, *J. Geophys. Res.*, *101*, 25,917–25,930, 1996.

Maenhaut, W., Composition and origin of the regional atmospheric aerosol at great distance from anthropogenic source areas, Assessment of the extent of the anthropogenic perturbation, final report, Fed. Off. for Sci., Tech., and Cult. Affairs, Brussels, Belg., 1997.

Maenhaut, W., and H. Raemdonck, Accurate calibration of a Si(Li) detector for PIXE analysis, *Nucl. Instrum. Method. Phys. Res.*, *1*, 123–136, 1984.

Maenhaut, W., and W. H. Zoller, Determination of the chemical composition of the south pole aerosol by instrumental neutron activation, *J. Radioanal. Chem.*, *37*, 637–650, 1977.

Maenhaut, W., A. Selen, P. Van Espen, R. Van Grieken, and J. W. Winchester, PIXE analysis of aerosol samples collected over the Atlantic Ocean from a sailboat, *Nucl. Instrum. Method.*, *181*, 399–405, 1981.

Maenhaut, W., I. Salma, J. Cafmeyer, H. J. Annegarn, and M. O. Andreae, Regional atmospheric aerosol composition and sources in the eastern Transvaal, South Africa, and impact of biomass burning, *J. Geophys. Res.*, *101*, 23,631–23,650, 1996a.

Maenhaut, W., R. Salomonovic, J. Cafmeyer, C. Ichoku, A. Karnieli, and M. O. Andreae, Anthropogenic and natural radiatively active aerosol types at Sede Boker, Israel, *J. Aerosol Sci.*, *27*, S47–S48, 1996b.

Maenhaut, W., J. Cafmeyer, J. Ptasinski, M. O. Andreae, T. W. Andreae, W. Elbert, F. X. Meixner, A. Karnieli, and C. Ichoku, Chemical composition and light scattering of the atmospheric aerosol at a remote site in the Negev desert, Israel, *J. Aerosol Sci.*, *28*, S73–S74, 1997.

Malm, W. C., L. T. Sisler, D. Kaufman, R. A. Eldred, and T. A. Cahill, Spatial and seasonal trends in particle concentrations and optical extinction in the United States, *J. Geophys. Res.*, *99*, 1347–1370, 1994.

Mason, B., and C. B. Moore, *Principles of Geochemistry*, 4th ed., John Wiley, New York, 1982.

Meszaros, E., A. Molnar, and J. Ogren, Scattering and absorption coefficients vs. chemical composition of fine atmospheric aerosol particles under regional conditions in Hungary, *J. Aerosol Sci.*, *29*, 1171–1178, 1998.

Nemesure, S., R. Wagener, and S. E. Schwartz, Direct shortwave forcing of climate by anthropogenic sulfate aerosol: Sensitivity to particle size, composition, and relative humidity, *J. Geophys. Res.*, *100*, 26,105–26,116, 1995.

Novakov, T., D. A. Hegg, and P. V. Hobbs, Airborne measurements of carbonaceous aerosols on the east coast of the United States, *J. Geophys. Res.*, *102*, 30,023–30,030, 1997.

Peleg, M., M. Luria, I. Setter, D. Perner, and P. Russell, Ozone levels in central Israel, *Isr. J. Chem.*, *34*, 375–386, 1994.

Penner, J. E., C. C. Chuang, and K. Grant, Climate forcing by carbonaceous and sulfate aerosols, *Clim. Dyn.*, *14*, 839–851, 1998.

Penner, J., R. Leaitch, D. Murphy, J. Nganga, and G. Pitari, Aerosols, their direct and indirect effects, in *Climate Change: The Scientific Basis*, edited by J. Houghton, Y. Ding, D. J. Griggs, M. Noguer, P. J. van der Linden, X. Dai, K. Maskell, and C. A. Johnson, pp. 289–348, Cambridge Univ. Press, New York, 2001.

Pham, M., J.-F. Müller, G. P. Brasseur, C. Granier, and G. Mégie, A three-dimensional study of the tropospheric sulfur cycle, *J. Geophys. Res.*, *100*, 26,061–26,092, 1995.

Pilinis, C., and X. Li, Particle shape and internal inhomogeneity effects on the optical properties of tropospheric aerosols of relevance to climate forcing, *J. Geophys. Res.*, *103*, 3789–3800, 1998.

Quinn, P. K., S. F. Marshall, T. S. Bates, D. S. Covert, and V. N. Kapustin, Comparison of measured and calculated aerosol properties relevant to the direct radiative forcing of tropospheric sulfate aerosol on climate, *J. Geophys. Res.*, *100*, 8977–8991, 1995.

Quinn, P. K., V. N. Kapustin, T. S. Bates, and D. S. Covert, Chemical and optical properties of marine boundary layer aerosol particles of the mid-Pacific in relation to sources and meteorological transport, *J. Geophys. Res.*, *101*, 6931–6951, 1996.

Schutyser, P., W. Maenhaut, and R. Dams, Instrumental neutron activation analysis of dry atmospheric fallout and rainwater, *Anal. Chem. Acta*, *100*, 75–85, 1978.

Schwartz, S. E., and M. O. Andreae, Uncertainty in climate change caused by aerosols, *Science*, *272*, 1121–1122, 1996.

Seinfeld, J. H., and S. N. Pandis, *Atmospheric Chemistry and Physics: From Air Pollution to Climate Change*, 1326 pp., John Wiley, New York, 1998.

Sheridan, P. J., and J. A. Ogren, Observations of the vertical and regional variability of aerosol optical properties over central and eastern North America, *J. Geophys. Res.*, *104*, 16,793–16,805, 1999.

Shine, K. P., and P. M. D. F. Forster, The effect of human activity on radiative forcing of climate change: A review of recent developments, *Global Planet. Change*, *20*, 205–225, 1999.

Sokolik, I. N., and O. B. Toon, Incorporation of mineralogical composition into models of the radiative properties of mineral aerosol from UV to IR wavelengths, *J. Geophys. Res.*, *104*, 9423–9444, 1999.

Stanhill, G., and S. Moreshet, Global radiation climate changes in Israel, *Clim. Change*, *22*, 121–138, 1992.

Tegen, I., and R. Miller, A general circulation model study of the interannual variability of soil dust aerosol, *J. Geophys. Res.*, *103*, 25,975–25,995, 1998.

Tegen, I., A. A. Lacis, and I. Fung, The influence on climate forcing of mineral aerosols from disturbed soils, *Nature*, *380*, 419–422, 1996.

ten Brink, H. M., S. E. Schwartz, and P. H. Daum, Efficient scavenging of the aerosol sulfate by liquid-water clouds, *Atmos. Environ.*, *21*, 2035, 1987.

ten Brink, H. M., J. P. Veefkind, A. Waijers-Ijpelaan, and J. C. van der Hage, Aerosol light-scattering in the Netherlands, *Atmos. Environ.*, *30*, 4251–4261, 1996.

Twomey, S., The influence of pollution on the short-wavde albedo of clouds, *J. Atmos. Sci.*, *34*, 1149–1152, 1977.

Vasconcelos, L. A. D. P., E. S. Macias, P. H. McMurry, B. J. Turpin, and W. H. White, A closure study of extinction apportionment by multiple regression, *Atmos. Environ.*, *35*, 151–158, 2001.

Waggoner, A. P., A. J. Vanderpol, R. J. Charlson, S. Larsen, L. Granat, and C. Tradgard, Sulfate light scattering ratio as an index of the role of sulfur in the tropospheric optics, *Nature*, *261*, 120–122, 1976.

Waggoner, A. P., A. P. Weiss, N. C. Ahlquist, D. S. Covert, and R. J. Charlson, Optical characteristics of atmospheric aerosols, *Atmos. Environ.*, *15*, 1891–1909, 1981.

Warren, S. G., C. J. Hahn, J. London, R. M. Chervin, and R. L. Jenne, Global distribution of total cloud cover and cloud type amounts over land, *NCAR Tech. Note, NCAR/TN-273*, Natl. Cent. for Atmos. Res., Boulder, Colo., 1986.

Wedepohl, K. H., *Geochemistry*, 231 pp., Holt, Rinehart, and Winston, Fort Worth, Tex., 1971.

White, W. H., On the theoretical and empirical basis for apportioning extinction by aerosols: A critical review, *Atmos. Environ.*, *20*, 1659–1672, 1986.

White, W. H., Contributions to light extinction, in *Visibility: Existing and Historical Conditions—Causes and Effects*, edited by J.C. Trijonis, W. C. Malm, M. Pitchford, W. H. White, R. Charlson, and R. Husar, *NAPAP Rep. 24*, pp. 85–102, Natl. Acid Precip. Assess. Program, Washington, D. C., 1990.

White, W. H., E. S. Macias, R. C. Nininger, and D. Schorran, Size-resolved measurements of light scattering by ambient particles in the Southwestern USA, *Atmos. Environ.*, *28*, 909–921, 1994.

M. O. Andreae and T. W. Andreae, Biogeochemistry Department, Max Planck Institute for Chemistry, P.O. Box 3060, 55020 Mainz, Germany. (moa@mpch-mainz.mpg.de)

C. Ichoku, Science Systems and Applications Inc., Climate and Radiation Branch, Code 913, NASA GSFC, Greenbelt, MD 20771, USA. (ichoku@climate.gsfc.nasa.gov)

A. Karnieli and L. Orlovsky, Jacob Blaustein Institute for Desert Research, Ben Gurion University of the Negev, Campus 84990, Sde Boker, Israel. (karnieli@bgumail.bgu.ac.il)

W. Maenhaut and J. Cafmeyer, Institute for Nuclear Sciences, University of Gent, Proeftuinstraat 86, B-9000 Gent, Belgium. (willy.maenhaut@rug.ac.be)